Magnetism of metallacrown single-molecule magnets: From a simplest model to realistic systems

Y. Pavlyukh,[1,2,*] E. Rentschler,[3] H. J. Elmers,[4] W. Hübner,[1] and G. Lefkidis[1]
[1]*Department of Physics and Research Center OPTIMAS, Technische Universität Kaiserslautern, P.O. Box 3049, 67653 Kaiserslautern, Germany*
[2]*Institut für Physik, Martin-Luther-Universität Halle-Wittenberg, 06120 Halle, Germany*
[3]*Institut für Anorganische und Analytische Chemie, Universität Mainz, D-55128 Mainz, Germany*
[4]*Institut für Physik, Johannes Gutenberg-Universität Mainz, D-55128 Mainz, Germany*

(Received 21 February 2018; revised manuscript received 17 May 2018; published 8 June 2018)

Electronic and magnetic properties of molecular nanomagnets are determined by competing energy scales due to the crystal field splitting, the exchange interactions between transition metal atoms, and relativistic effects. We present a comprehensive theory embracing all these phenomena based on first-principles calculations. In order to achieve this goal, we start from the $FeNi_4$ cluster as a paradigm. The system can be accurately described on the *ab initio* level yielding all expected electronic states in a range of multiplicities from 1 to 9, with a ferromagnetic ground state. By adding the spin-orbit coupling between them we obtain the zero-field splitting. This allows to introduce a spin Hamiltonian of a giant spin model, which operates on a smaller energy scale. We compare the computed parameters of this Hamiltonian with the experimental and theoretical magnetic anisotropy energies of the monolayer Ni/Cu(001). In line with them, we find that the anisotropy almost entirely originates from the second-order spin-orbit coupling, the spin-spin coupling constitutes only a small fraction. Finally, we include the ligand atoms in our consideration. This component has a decisive role for the stabilization of molecules in experimental synthesis and characterization, and also substantially complicates the theory by bringing the superexchange mechanisms into play. Since they are higher-order effects involving two hopping matrix elements, not every theory can describe them. Our generalization of the corresponding perturbation theory substantiates the use of complete active space methods for the description of superexchange. At the same time, our numerical results for the $\{CuFe_4\}$ system demonstrate that the Goodenough-Kanamori rules, which are often used to determine the sign of these exchange interactions, cannot deliver quantitative predictions due to the interplay of other mechanisms, e. g., involving multicenter Coulomb integrals. We conclude by comparing *ab initio* values of the exchange interaction constants for the $\{CuCu_4\}$ and $\{CuFe_4\}$ metallacrown magnetic molecules with experimental values determined by fitting of the magnetic susceptibility curves $\chi_M T(T)$, and attribute the remaining discrepancy between them to the role of virtual electron excitations into and out of the active space (dynamical correlations).

DOI: 10.1103/PhysRevB.97.214408

I. INTRODUCTION

Spin models are fundamental paradigms of condensed matter physics, yielding a rich family of magnetically ordered phases [1,2], realized in physically very diverse systems by a number underlying mechanisms. In this work, we focus on the question to which extent these spin model Hamiltonians can be applied to finite molecular systems [3,4], and present a comprehensive theory for treating realistic molecules such as metallacrowns [5,6]. This class of organometallic molecular systems features a remarkable diversity of compositions, spin states and physical properties [7–10]. It typically comprises a cyclic arrangement of four ring metal ions and hosts another metal guest ion at its core. Metallacrowns (MC) are excellent candidates for observations of the slow relaxation of the magnetization—in contrast to quantum tunneling [11,12]. This process is often rationalized in terms of the giant spin model [13–16], which on the one hand justifies the term single-molecule magnet (SMM) [17–19], and on the other hand poses the question as to what extent such a macrospin scenario is relevant: for instance it is known that the giant spin model is inadequate when different spin multiplets are nested within the ground state [20].

Thus, one prominent question for any theory is to determine the validity range of different spin models, notably supported by *ab initio* calculations. There is no general prescription here: the constituent transition metal (TM) atoms offer great flexibility in the occupation of 3*d* orbitals and can lead to a low- or high-spin ground-state configuration depending on the choice of atoms and ligand (donor) atoms. Thus the analysis needs to be specifically performed for each system. To this end, we consider here a series of systems ranging from the simplest five-center transition metal cluster to recently synthesized $Cu^{II}(DMF)_2Cl_2[12{-}MC_{Fe^{III}N(Shi)}-4](DMF)_4$ and $(HNEt_3)_2Cu^{II}[12{-}MC_{Cu^{II}N(Shi)}-4]$ metallacrowns ($\{CuFe_4\}$ and $\{CuCu_4\}$ for brevity; in the full metallacrown notation, as introduced by Pecoraro, 12 refers to the total number of segments in the cyclic host, and 4 is the number of involved oxygen atoms [7,9]) (Fig. 1). We demonstrate how corresponding spin models can be constructed on each stage and aligned with experimental measurements of magnetic susceptibility,

*pavlyukh@physik.uni-kl.de

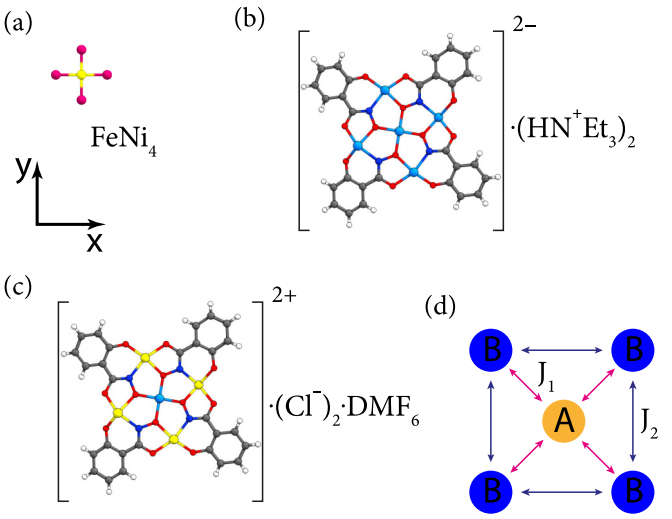

FIG. 1. (a)–(c) The three systems of the present study and (d) a generic spin model. *Ab initio* calculations are performed on the $FeNi_4$ cluster (a), and on the charged minimal models of metallacrowns [(b) and (c)]. They are constructed by depriving MCs of weakly bound solvent molecules and coordinated anions ($HNEt_3$, DMF, Cl^-), and have a form AB_4L_4, where A and B are TM atoms. Notice that Ni (d^9) in $FeNi_4$ is isoelectronic with Cu^{II} in $\{CuCu_4\}$ (b) and $\{CuFe_4\}$ (c), and therefore these systems can be used for comparison. Color scheme: light blue, yellow, and magenta spheres stand for Cu, Fe, and Ni transition metal atoms, respectively. C, N, and O atoms are depicted as grey, blue, and red spheres, respectively. Hydrogen atoms have been removed for clarity. All three systems (a)–(c) are shown on the same scale. DMF stands for dimethylformamide, and L=$C_7H_4NO_3$ is the ligand complex.

x-ray magnetic circular dichroism measurements of element-selective magnetic moments [21], and high-field electron paramagnetic resonance (EPR) measurements [22] of the axial (D) and rhombic (E) zero-field splitting (ZFS) [23] parameters. The manuscript is thus divided into three sections describing the first-principles calculations and their applications to $FeNi_4$ and $\{CuCu_4\}$, $\{CuFe_4\}$. The bare metallic $FeNi_4$ cluster enables us to perform extended calculations, which are prohibitively complicated for the metallacrown molecules involving large organic moities. At the same time, Ni (d^9) in $FeNi_4$ is isoelectronic with Cu^{II} in $\{CuCu_4\}$ and $\{CuFe_4\}$ allowing for the comparison of direct and ligand-mediated exchange mechanisms and for the investigation of relativistic effects.

While generally a very accurate correspondence between our *ab initio* calculations and a spin model can be established, our main goal is to explain the remaining discrepancies. Qualitative understanding is provided by the Goodenough-Kanamori rules. However, being based on perturbation theory, the rules are not accurate enough to make quantitative predictions. This is rigorously shown for the $\{CuCu_4\}$ and $\{CuFe_4\}$ metallacrown systems.

As we said above, the studied systems are at the intersection of several fields: physical chemistry, theoretical solid state physics, and quantum chemistry (Fig. 2). For instance, the zero-field splitting in molecular systems is regarded as the magnetic anisotropy in solid state materials. The Hubbard U can be perceived as a parameter in some of the models, or it can be computed from first principles, or determined by the fitting

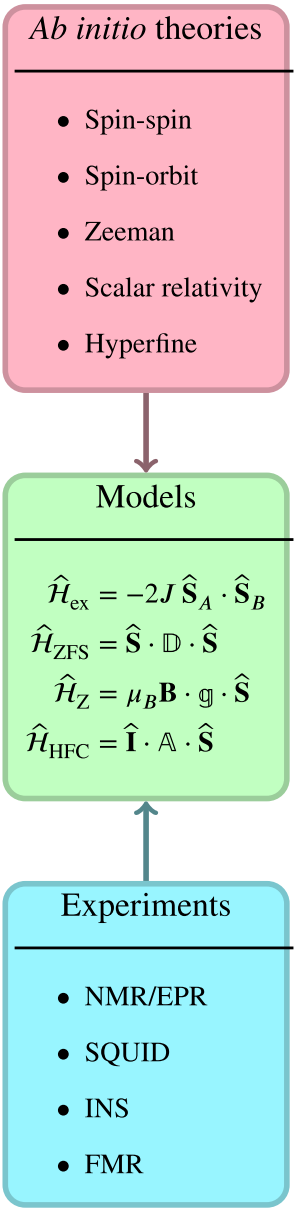

FIG. 2. Outline of this work. We specifically focus on the Heisenberg-Dirac-Van Vleck Hamiltonian $\hat{\mathcal{H}}_{ex}$ and the zero-field splitting Hamiltonian $\hat{\mathcal{H}}_{ZFS}$ bridging our *ab initio* calculations and experimental measurements. Other abbreviations are NMR/EPR (nuclear magnetic resonance/electron paramagnetic resonance), SQUID (superconducting quantum interference device), INS (inelastic neutron scattering), and FMR (ferromagnetic resonance). $\hat{\mathcal{H}}_Z$ denotes the Zeeman Hamiltonian, whereas $\hat{\mathcal{H}}_{HFC}$ is the hyperfine coupling Hamiltonian.

of atomic spectroscopy data. Therefore the paper is organized as to bridge these communities and to provide a unifying view on the topic. Theoretical concepts used in this work are presented in Sec. II, which is divided into three subsections: the first-principles calculations including relativistic effects (Sec. II A), Hamiltonians of the spin models (Sec. II B), and the computation of experimental observables such as magnetic susceptibilities (Sec. II C). Our main results are presented in Sec. III, which is devoted to the bare metallic $FeNi_4$ cluster, and in Sec. IV devoted to the two metallacrowns. In Appendix A

we summarize *ab initio* methods used in this work and in Appendix B we investigate the role of biquadratic exchange interactions.

II. THEORY

A. First-principles calculations

Ab initio calculations in this work were performed using the complete active space (CAS) and correlated methods as implemented in the ORCA quantum chemistry program [24]. These results can either be directly interpreted in terms of energies and spin expectation values or used to produce hopping t_{ij} and Coulomb matrix elements $\langle ij|1/r|kl\rangle$. They are the ingredients of a general many-body Hamiltonian

$$\hat{\mathcal{H}} = \sum_{ij} t_{ij\sigma}\hat{c}^{\dagger}_{i\sigma}\hat{c}_{j\sigma} + \frac{1}{2}\sum_{ijkl}\sum_{\sigma\sigma'}\langle ij|1/r|kl\rangle\hat{c}^{\dagger}_{i\sigma}\hat{c}^{\dagger}_{j\sigma'}\hat{c}_{l\sigma'}\hat{c}_{k\sigma}, \tag{1}$$

where i, j, k, l specify the spatial state and $\sigma,\sigma' = \pm 1$ are the spin labels. Here and in what follows (unless explicitly specified) we use atomic units ($m_e = e = \hbar = 4\pi\varepsilon_0 = 1$). Exact diagonalization (ED) of this Hamiltonian is only feasible for very small active spaces. However, since we are interested only in magnetic excitations, which are close to the ground state and because the systems of interest permit a description in terms of the localized basis states, their spectrum can efficiently be computed within the density matrix renormalization group (DMRG) approach. We are using the CHEMPS2 [25] implementation for this purpose.

The hopping t_{ij} contains the electron kinetic energy, the interaction with nuclei, and the mean-field Coulomb part. It is important to emphasize that already for $3d$ transition metal atoms relativistic effects [26] are important. The scalar-relativistic effects are included via the second-order Douglas-Kroll-Hess (DKH) transformation [27] and are incorporated in the hopping matrix elements.

The spin-orbit

$$\hat{\mathcal{H}}_{\mathrm{SOC}} = \frac{\alpha^2}{2}\sum_i\sum_A Z_A\frac{(\mathbf{r}_i - \mathbf{R}_A)\times\mathbf{p}_i}{|\mathbf{r}_i - \mathbf{R}_A|^3}\hat{\mathbf{s}}_i - \frac{\alpha^2}{2}\sum_i\sum_{j\neq i}\frac{(\mathbf{r}_i - \mathbf{r}_j)\times\mathbf{p}_i}{|\mathbf{r}_i - \mathbf{r}_j|^3}(\hat{\mathbf{s}}_i + 2\hat{\mathbf{s}}_j) \tag{2}$$

and the spin-spin

$$\hat{\mathcal{H}}_{\mathrm{SSC}} = \frac{\alpha^2}{2}\sum_i\sum_{j\neq i}\frac{1}{|\mathbf{r}_i - \mathbf{r}_j|^3}\left[\hat{\mathbf{s}}_i\cdot\hat{\mathbf{s}}_j - \frac{3(\hat{\mathbf{s}}_i\cdot\mathbf{r}_{ij})(\hat{\mathbf{s}}_j\cdot\mathbf{r}_{ij})}{|\mathbf{r}_i - \mathbf{r}_j|^2}\right] \tag{3}$$

couplings (SSC) are added perturbatively. Here, $\mathbf{r}$, $\mathbf{p}$, and $\hat{\mathbf{s}}$ are position, momentum, and spin operators of an electron, $\alpha = 1/c$ is the fine-structure constant. There is no contact SSC term for electrons [28].

The spin-spin coupling is a prototypic microscopic mechanism of the so-called magnetic shape anisotropy [29,30]. Whereas the first term in Eq. (3) depends only on the mutual orientation of spins and favors their antiferromagnetic alignment, the second term depends on the relative orientation of spins and a vector between them, $\mathbf{r}_{ij}$. Therefore, it is sensitive to the geometry of a sample: vanishes for the infinite-sized crystals and favors the in-plane alignment in thin films. In the latter case, a sum over the lattice can be performed yielding for magnetic moments m located at lattice sites with period a and ferromagnetically aligned at angle ϕ to the surface normal the energy $E = \frac{1}{2}\frac{\mu_0}{a^3}m^2\cos^2\phi$ [31,32]. In more complicated geometries, the geometrical parameters are conventionally parametrized in terms of the demagnetizing factors [33].

B. Spin models

In full generality, effective spin models are simplifications, which arise by projecting out irrelevant energy scales. By focusing on the lowest energy spin multiplet $|aS_a\rangle$ and neglecting the exchange interactions with other spins or nuclei, the following spin Hamiltonian defined in terms of the $\mathbb{g}$ and $\mathbb{D}$ tensors is relevant:

$$\hat{\mathcal{H}}_{\mathrm{S}} = \mu_B\mathbf{B}\cdot\mathbb{g}\cdot\hat{\mathbf{S}} + \underbrace{\hat{\mathbf{S}}\cdot\mathbb{D}\cdot\hat{\mathbf{S}}}_{\hat{\mathcal{H}}_{\mathrm{ZFS}}}. \tag{4}$$

This is the most general form of an interaction of spins with a magnetic field $\mathbf{B}$, *linear* in $\mathbf{B}$ and $\hat{\mathbf{S}}$, and a *bilinear* interaction of spins and can simultaneously be regarded as the definition of corresponding $\mathbb{g}$ and $\mathbb{D}$ tensors. While this form arises from the Dirac-Coulomb-Breit Hamiltonian [28], two important parts of which are given by Eqs. (2) and (3), it is also used for more general scenarios. For instance, the magnetic field $\mathbf{B}$ in the Zeeman interaction (first term) can be applied externally or arise as exchange bias at interfaces, in magnetic heterostructures [34,35]. For the first part, relativistic-mass correction, paramagnetic and diamagnetic terms of the Breit-Pauli Hamiltonian introduce important corrections to the $\mathbb{g}$ tensor, which are further modified by the external magnetic field [27]. The second term contains relativistic effects leading to the splitting of the multiplet even in the absence of the field. This part is also known as the zero-field splitting (ZFS) Hamiltonian $\mathcal{H}_{\mathrm{ZFS}}$. It is the cause of the magnetic anisotropy, and has profound effects on magnetic properties. For example, magnetic hardness (the width of a hysteresis loop) is determined by the magnitude of $\mathbb{D}$. As for the origin of ZFS, if $\hat{\mathcal{H}}_{\mathrm{SOC}}$ and $\hat{\mathcal{H}}_{\mathrm{SSC}}$ are treated perturbatively, it consists of a first-order term arising from the direct spin-spin interaction (3) and of a second-order contribution from the spin-orbit coupling, Eq. (2). We notice that $\hat{\mathcal{H}}_{\mathrm{SOC}}$ yields splittings of the ground-state multiplet already in the first order, however, its form is not bilinear in spin operators as postulated by the general form (4). A standard way to find the $\mathbb{D}$ tensor is to equate the matrix elements of the first principles, $\hat{\mathcal{H}}_{\mathrm{SOC}} + \hat{\mathcal{H}}_{\mathrm{SSC}}$, and the model $\hat{\mathcal{H}}_{\mathrm{ZFS}}$ Hamiltonians:

$$\langle aS_aM|\hat{\mathcal{H}}_{\mathrm{ZFS}}|aS_aM'\rangle = \langle aS_aM|\hat{\mathcal{H}}_{\mathrm{SSC}}|aS_aM'\rangle + \sum_{b,M''}\frac{\langle aS_aM|\hat{\mathcal{H}}_{\mathrm{SOC}}|bS_bM''\rangle\langle bS_bM''|\hat{\mathcal{H}}_{\mathrm{SOC}}|aS_aM'\rangle}{E_a - E_b}. \tag{5}$$

According to the selection rules for the spin-orbit coupling, the computation of the second-order term involves a sum over the intermediate states $|bS_b\rangle$ with $S_b - S_a = 0, \pm 1$, as detailed

by Neese [36], different implementations are compared by van Wüllen *et al.* [37,38]. While $\hat{\mathcal{H}}_{\rm ZFS}$ can be generally put in correspondence with magnetic anisotropy energy (MAE) of an extended system (comprising the magnetocrystalline and the shape parts), there are important differences how they are evaluated in practice. Focusing on the magnetocrystalline part, there are a lot of intricacies related to the bulk versus interface contributions, which are very sensitive to the underlying crystal structure [30,39,40]. Nonetheless, the second-order dependence of the energy on the spin-orbit coupling is predicted [41]. While this is natural in view of the microscopic expression (5), in the case of band-structure calculations of extended systems, special treatment is required for degenerate states and band-crossings [31,32,42].

On a larger energy scale, the interaction of spins on different sites needs to be taken into account. On the basis of Eqs. (2) and (3), relativistic effects rapidly subdue with the distance as reflected in the well known fact that the spin-other orbit coupling is weak. However, the Pauli exclusion principle is still operative and governs exchange interactions. Transition metals are known for the importance of the orbital degrees of freedom, which manifest themselves in the ordering of the orbitals. For example, it is typical in solid state physics to represent the e_g and t_{2g} states in tetrahedral or octahedral crystal environments as pseudospins with momentum $1/2$ and 1, respectively. Following Tokura and Nagaosa [43], a generic Hamiltonian would be

$$\mathcal{H}_{\rm PS} = \sum_{ij}[J_{ij}(\hat{\mathbf{T}}_i,\hat{\mathbf{T}}_j)\hat{\mathbf{S}}_i\cdot\hat{\mathbf{S}}_j + K_{ij}(\hat{\mathbf{T}}_i,\hat{\mathbf{T}}_j)]. \tag{6}$$

The interaction between spins $\hat{\mathbf{S}}$ and pseudospins $\hat{\mathbf{T}}$, which is not necessarily of relativistic origin as Eqs. (2) and (3), sets all the multitude of electronic levels, whereas magnetic properties are determined solely by the spin configuration. The form of the Hamiltonian (6) is not unique and stresses the spin degrees of freedom. First-principles determination of the exchange constants J_{ij} and K_{ij} is a daunting task [44]. This becomes evident considering the fact that even in two-spin systems in the absence of orbital degrees of freedom, there are at least three approaches differing by the correction $\Delta_{\rm S}$ for the determination of a single J parameter on the basis of the energy difference between the high- (HS) and the low-spin (LS) configurations [45]:

$$J = \frac{E_{\rm LS} - E_{\rm HS}}{\langle\hat{\mathbf{S}}^2\rangle_{\rm HS} - \Delta_{\rm S}}. \tag{7}$$

In the present work, we will focus on the spin-only Hamiltonian as discussed below. However, we will see examples where this model is insufficient.

For a square planar AB_4 molecule schematically depicted in Fig. 1 the isotropic exchange (ex) Heisenberg-Dirac-Van Vleck Hamiltonian [4] is given by

$$\hat{\mathcal{H}}_{\rm ex} = -2J_1\sum_i \hat{\mathbf{s}}_A\cdot\hat{\mathbf{s}}_{B_i} - 2J_2\sum_{\langle ij\rangle}\hat{\mathbf{s}}_{B_i}\cdot\hat{\mathbf{s}}_{B_j}, \tag{8}$$

where $\langle ij\rangle$ denotes a collection of nearest neighbors. $\hat{\mathbf{s}}_A$ and $\hat{\mathbf{s}}_{B_i}$ are effective spin operators representing possibly composite spins on the centers A and B_i, respectively. The exchange constants $J_{1,2}$ are positive for ferromagnetic (FM) interactions and negative for antiferromagnetic (AFM) ones. As a possible generalization, a biquadratic interaction between spins can be considered, i.e., $\hat{\mathcal{H}}^{(2)}_{\rm ex}$, where

$$\hat{\mathcal{H}}^{(2)}_{\rm ex} = -\kappa_1\sum_i(\hat{\mathbf{s}}_A\cdot\hat{\mathbf{s}}_{B_i})^2 - \kappa_2\sum_{<ij>}(\hat{\mathbf{s}}_{B_i}\cdot\hat{\mathbf{s}}_{B_j})^2. \tag{9}$$

For our systems, κ_1 and κ_2 are very small. Interactions between the next nearest neighbors (along diagonals) are neglected because there is no effective coupling mechanism. Some authors, notably Kahn in Ref. [3], define the Heisenberg-Dirac-Van Vleck Hamiltonian with different prefactors. In what follows, we adhere to definition (8), which is also consistent with the review of Furrer and Waldmann [4].

In addition to indirect mechanisms that will be considered in details below, the bare Coulomb interaction between molecular orbitals

$$\begin{aligned}\langle ij|1/r|kl\rangle &= \int d\mathbf{r}\int d\mathbf{r}'\,\frac{\phi_i^*(\mathbf{r})\phi_j^*(\mathbf{r}')\phi_k(\mathbf{r}')\phi_l(\mathbf{r})}{|\mathbf{r}-\mathbf{r}'|}\\ &\equiv (il|kj)\end{aligned} \tag{10}$$

is a possible microscopic origin of exchange interactions. The matrix elements are typically categorized into Hubbard U and exchange J interactions, which nonetheless result from the same four-index quantity. The dominant ones are those having at most two distinct indices and having a generic form

$$U_{ab} \equiv (aa|bb), \quad J_{ab} \equiv (ab|ab). \tag{11}$$

They were specifically considered by Hubbard in the well known model of Ref. [46]. As a side remark, there are a lot of intricacies of this parametrization in the atomic limit, where U and J can be determined from atomic spectroscopy data as clarified by Hübner and Falicov [47]: the spherical symmetry can only be assured by the inclusion of four-index quantities, in cubic environment the exchange anisotropy term ΔJ given in the TM ions by the $e_g{-}t_{2g}$ splitting is important, etc. While these are key quantities in the crystal field models, they attain their second life in the density functional calculations using the LDA+U approach [48]. Here, for us it will be important to notice that depending on whether a and b are centered on the same atom, nearest neighbors, or across the diagonal, the magnitude of U and J can span the range from tens of eV to μeV [49,50]. However, they are always positive and cannot explain that interactions between spins on TM atoms bridged by several organic atoms can be rather large and not necessarily ferromagnetic. Therefore, as we mentioned above, in the majority of systems including bulk materials and molecular magnets, the dominant contribution to the exchange constants is from indirect mechanisms: either mediated by intermediate atoms (superexchange), or facilitated by the hopping between two neighboring atoms (kinetic exchange) [51]. The systems considered here exemplify this point: the central TM atom (A) in metallacrowns [Figs. 1(b) and 1(c)] is bound indirectly via an oxygen (A–O–B) or an oxamate bridge (A–O–N–B) to the TM atoms on the ring (B). The interaction between ring atoms is also mediated by the oxamate bridge (B–O–N–B). This is to be contrasted with the $FeNi_4$ cluster that possesses direct bonds, Fig. 1(a).

Of relevance for the studied systems (Fig. 1) are superexchange mechanisms (see Ref. [52]): while the $FeNi_4$ cluster

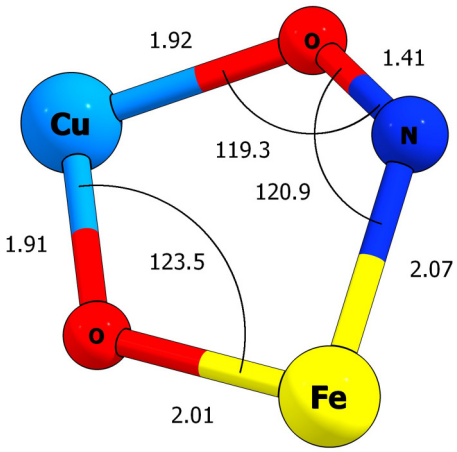

FIG. 3. Bond lengths (Å) and angles (degrees) of a central fragment of the $Cu^{II}[12-MC_{Fe^{III}N(Shi)}-4]$ metallacrown. Simplistic application of the Goodenough-Kanamori rule predicts that the magnetic interactions between Cu^{II} and Fe^{III} ions are antiferromagnetic when electrons can hop between the d orbitals of TM ions via the p_z orbital of O. In the opposite case, when the Fe–O–Cu angle approaches 90°, such hopping is not possible. In this case, a ferromagnetic interaction arises due to the hopping of d-electrons onto two orthogonal p orbitals.

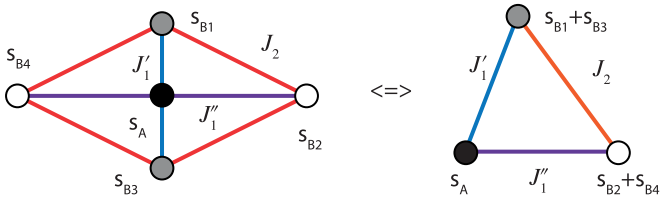

FIG. 4. Correspondence between the rhombically distorted AB_4 spin system and a spin triangle. Analytic solution is possible for $S_A = 1/2$ and is given by Eq. (12).

lacks ligand-mediated pathways, the indirect mechanisms are still operative there; at variance, the $\{CuCu_4\}$ and the $\{CuFe_4\}$ metallacrowns are paradigmatic examples. Consider for instance the A–O–B bond. When the d orbitals on A and B interact via an oxygen in-between (in the linear geometry), both d orbitals couple to the same p_z orbital, while the hopping to the two other p_x and p_y orbitals vanishes by symmetry. The result is an antiferromagnetic superexchange coupling which is due to the unobstructed electron-hopping via the oxygen p_z bridge and the on-site Hubbard repulsion. When the A–O–B angle is close to 90°, the d orbitals couple to two orthogonal p_x/p_y orbitals, making it impossible for an electron on one d orbital to reach the d orbital on the other site. In this case, the superexchange is mediated via the *intraatomic* Coulomb exchange on oxygen, and is ferromagnetic. Each of the operative mechanisms depend in a crucial way on the occupation of the participating orbitals. This is the rationale behind the so-called Goodenough-Kanamori rules [53–55]. We refer here to the excellent monograph (Sec. III B) by John B. Goodenough [56] for the discussion of all intricacies. In realistic molecular systems, there is no clear separation between the two mechanisms as evidenced by Fig. 3.

Biquadratic spin interactions (9) are typically associated with magnetoelastic mechanisms as was originally proposed by Kittel [57] and found in experiments on, e.g., spinels [58], or even on the Ni_4 magnetic molecules [59]. However, it may also be obtained from the many-body Hamiltonian via an indirect mechanism as was indicated by P .W. Anderson [60,61]. In fact, the lowest-order contribution to the biquadratic exchange constant κ is the same as in the antiferromagnetic exchange mechanism, i.e., proportional to the forth power of the hopping between the magnetic d orbitals and the ligand p orbitals, and inversely proportional to the third power of the on-site Coulomb repulsion. This is not surprising given the fact that $(\hat{\mathbf{s}}_i \cdot \hat{\mathbf{s}}_j)^2 = \frac{3}{16} - \frac{1}{2}(\hat{\mathbf{s}}_i \cdot \hat{\mathbf{s}}_j)$ for $s_i = s_j = \frac{1}{2}$, and therefore it makes sense to introduce the biquadratic exchange only for higher spins [62]. In Appendix B, we generalize this trick to spin triangles of the type AB_2, where only $s_A = \frac{1}{2}$. This is relevant for our discussion of subsystems of spin of the $\{CuFe_4\}$ metallacrown in Sec. IV B.

Regardless of the microscopic mechanisms, Eq. (8) can be solved analytically. Straightforwardly, but perhaps not widely known, even in the case of a rhombic distortion, the system can be mapped onto the Hamiltonian of a general spin triangle with spins $\hat{\mathbf{s}}_A$, $\hat{\mathbf{S}}_{B_1} = \hat{\mathbf{s}}_{B_1} + \hat{\mathbf{s}}_{B_3}$, and $\hat{\mathbf{S}}_{B_2} = \hat{\mathbf{s}}_{B_2} + \hat{\mathbf{s}}_{B_4}$, respectively, and three distinct exchange constants $J_1' = (1-\delta)j$, $J_1'' = (1+\delta)j$, and $J_2 = \alpha j$, as is shown in Fig. 4. In these notations, for arbitrary S_{B_i} and a fixed value of $s_A = 1/2$, the eigenenergies can be written in a concise form as functions of the total spin (S):

$$E(S) = -(S+1/2)^2\alpha j \pm j\sqrt{(S+1/2)^2(1-\alpha)^2 + [(S_{\max}+1/2)^2 - (S+1/2)^2]\delta^2}. \quad (12)$$

For a given total spin $S_{\min} \leqslant S \leqslant S_{\max} - 1$, there are two possible eigenvalues corresponding to ferromagnetic and antiferromagnetic alignments of the $\hat{\mathbf{S}}_{B_1}$ and $\hat{\mathbf{S}}_{B_2}$ spins. For antiferromagnetic coupling constant j, the plus sign in Eq. (12) corresponds to the lower antiferromagnetic branch of solutions. The upper branch has one additional eigenvalue corresponding to the ferromagnetic configuration and having the maximal spin $S_{\max} = s_A + S_{B_1} + S_{B_2}$. Some partial cases of this equation were considered by Haraldsen *et al.* [63].

For a square-symmetric system, the solution simplifies significantly and the energies can be given in terms of the total spin $\hat{\mathbf{S}} = \hat{\mathbf{s}}_A + \hat{\mathbf{S}}_B$, and three additional quantum numbers: $\hat{\mathbf{S}}_{13} = \hat{\mathbf{s}}_{B_1} + \hat{\mathbf{s}}_{B_3}$, $\hat{\mathbf{S}}_{24} = \hat{\mathbf{s}}_{B_2} + \hat{\mathbf{s}}_{B_4}$, and the total spin of the ring atoms $\hat{\mathbf{S}}_B = \hat{\mathbf{S}}_{13} + \hat{\mathbf{S}}_{24}$. The eigenstates are $|S_{13}S_{24}S_B S M_S\rangle$ and the corresponding energy is

$$E = -J_1[S(S+1) - s_A(s_A+1) - S_B(S_B+1)] - J_2[S_B(S_B+1) - S_{13}(S_{13}+1) - S_{24}(S_{24}+1)], \quad (13)$$

where $S_k(S_k+1)$ is the expectation value of $\hat{\mathbf{S}}_k^2$, and M_S is the total spin projection. The system is degenerate with respect to this quantum number. The dimension of the Hilbert space is

$(2s_A+1)(2S_B+1)^4$. Spin states for $s_A=2$ and $s_B\equiv s_{B_i}=\frac{1}{2}$ (with relevance for the $FeNi_4$ bare metallic cluster—its electronic configuration is analyzed in Sec. III) are decomposed as follows:

$$2\otimes\left[\tfrac{1}{2}\otimes\tfrac{1}{2}\otimes\tfrac{1}{2}\otimes\tfrac{1}{2}\right]=0\oplus 1^4\oplus 2^6\oplus 3^4\oplus 4, \tag{14}$$

where $S_A\otimes S_B$ and $S_A\oplus S_B$ is a direct product and a direct sum of two spin-representations of dimensions $2S_A+1$ and $2S_B+1$, respectively. The superscript specifies the number of independent multiplets of each spin.

Similarly, for the $\{CuCu_4\}$ and $\{CuFe_4\}$ metallacrowns with $s_B=\frac{1}{2},1,\frac{3}{2}$ and $s_A=\frac{1}{2}$ (their electronic configuration is analyzed in Sec. IV) the decomposition is as follows:

$$\tfrac{1}{2}\otimes\left[\tfrac{1}{2}\otimes\tfrac{1}{2}\otimes\tfrac{1}{2}\otimes\tfrac{1}{2}\right]=\tfrac{1}{2}^5\oplus\tfrac{3}{2}^4\oplus\tfrac{5}{2}, \tag{15a}$$

$$\tfrac{1}{2}\otimes\left[\tfrac{3}{2}\otimes\tfrac{3}{2}\otimes\tfrac{3}{2}\otimes\tfrac{3}{2}\right]=\tfrac{1}{2}^{13}\oplus\tfrac{3}{2}^{20}\oplus\tfrac{5}{2}^{21}\oplus\tfrac{7}{2}^{16}\oplus\tfrac{9}{2}^{9}\oplus\tfrac{11}{2}^{4}\oplus\tfrac{13}{2}, \tag{15b}$$

$$\tfrac{1}{2}\otimes\left[\tfrac{5}{2}\otimes\tfrac{5}{2}\otimes\tfrac{5}{2}\otimes\tfrac{5}{2}\right]=\tfrac{1}{2}^{21}\oplus\tfrac{3}{2}^{36}\oplus\tfrac{5}{2}^{45}\oplus\tfrac{7}{2}^{48}\oplus\tfrac{9}{2}^{45}\oplus\tfrac{11}{2}^{36}\oplus\tfrac{13}{2}^{25}\oplus\tfrac{15}{2}^{16}\oplus\tfrac{17}{2}^{9}\oplus\tfrac{19}{2}^{4}\oplus\tfrac{21}{2}. \tag{15c}$$

C. Thermodynamic properties

From the knowledge of the eigenstates, basic thermodynamic properties can be obtained. They are the partition function

$$Z=\sum_\lambda \exp\left(-\frac{E_\lambda}{k_BT}\right), \tag{16}$$

the magnetization along the α direction ($\alpha=x,y,z$):

$$M_\alpha=-g\mu_B\sum_\lambda p_\lambda\langle\lambda|\hat{S}_\alpha|\lambda\rangle, \tag{17}$$

and the magnetic susceptibility

$$\chi_{\alpha\alpha}=\frac{(g\mu_B)^2}{k_BT}\left[\sum_\lambda p_\lambda\langle\lambda|\hat{S}_\alpha^2|\lambda\rangle-\left(\sum_\lambda p_\lambda\langle\lambda|\hat{S}_\alpha|\lambda\rangle\right)^2\right], \tag{18}$$

where p_λ is the probability of thermally populating the state $\lambda\equiv|S_{13}S_{24}S_BSM_S\rangle$:

$$p_\lambda=\frac{1}{Z}\exp\left(-\frac{E_\lambda}{k_BT}\right).$$

Typically, we consider the magnetization along the z direction, which allows to perform the sum over $-S\leqslant M_S\leqslant S$, the degenerate substates:

$$\sum_\lambda p_\lambda\langle\lambda|\hat{S}_z^2|\lambda\rangle\equiv\frac{1}{Z}\sum_S\sum_{S_B}\sum_{S_{13}}\sum_{S_{24}}\exp\left(-\frac{E(S_{13}S_{24}S_BS)}{k_BT}\right)\times\sum_{M_S=-S}^{S}\langle M_S|\hat{S}_z^2|M_S\rangle, \tag{19}$$

TABLE I. Comparison of SI and cgs-emu units used in this work.

Quantity	SI	cgs-emu
Energy	J	1 erg=10^{-7} J
Magnetic field	T	1 G =10^{-4} T
Magnetization	J/T	erg/G
Bohr magneton μ_B	9.274×10^{-24} J/T	9.274×10^{-21} erg/G
Boltzmann constant k_B	1.381×10^{-23} J/K	1.381×10^{-16} erg/K
$N_A\mu_B^2/(3k_B)$		0.125 $cm^3\,mol^{-1}\,K$

and use hereby

$$\sum_{M_S=-S}^{S}\langle M_S|\hat{S}_z^2|M_S\rangle=\frac{1}{3}S(S+1)(2S+1). \tag{20}$$

Because $\sum_{M_S=-S}^{S}\langle M_S|\hat{S}_z|M_S\rangle=0$, the magnetization M_z (17) is zero. When spin-orbit coupling is included, the degeneracy is lifted and M_z need not be zero in general.

The magnetic susceptibility defined by Eq. (18) describes the response of a single molecule to the applied magnetic field, i.e., $\chi_{\alpha\alpha}=\frac{\partial M_\alpha}{\partial B_\alpha}$. In experiment, one averages over an ensemble of molecules, and the *molar* magnetic susceptibility $\chi_M=N_A\chi_{zz}$ is measured. Here, the magnetic field is in Gauss units (1G=10^{-4}T), Table I. The function $\chi_MT(T)$ is used for fitting.

One can obtain the low- and high-temperature limits by directly exploiting the Hilbert space partitions (15). At zero temperature there is a vanishing probability to occupy all but the ground state ($p_0=1$), whereas in the high-temperature limit $\exp(-\frac{E_\lambda}{k_BT})\sim1$ and $p_\lambda=1/Z$. In both cases, the susceptibility can be written in the same form, however, the values of the effective spin squared $\langle S^2\rangle$ differ:

$$\chi_MT(T)\sim\frac{N_A\mu_B^2}{3k_B}\langle S^2\rangle g^2, \tag{21}$$

$$\langle S^2\rangle_0=S_0(S_0+1), \tag{22}$$

$$\langle S^2\rangle_\infty=\frac{\sum_S\nu_SS(S+1)(2S+1)}{\sum_S\nu_S(2S+1)}, \tag{23}$$

where S_0 is the total spin of the ground state, and ν_s is the number of distinct spin multiplets S [they are indicated as exponents in Eqs. (15)]. For the three different choices of s_B, the values of the effective spin squared $\langle S^2\rangle_\infty$ are 15/4, 63/4, and 143/4. From these simple estimates, one can already make some useful conclusions. It is known that in $CuCu_4$ each of the copper atoms has one unpaired electron, $s_A=s_B=1/2$. Assuming a frustrated antiferromagnetic ground state with the total spin 1/2, we obtain by virtue of Eq. (21), 0.375 and 1.875 $cm^3mol^{-1}K$ for the low- and high-temperature limits of $\chi_MT(T)$, respectively.

These considerations cannot provide the susceptibility at intermediate temperatures, however, in some simple cases such as a single effective spin J, the exact analytic solution for the magnetization is given in terms of the Brillouin function

$M_z = Ng\mu_B J B_J(x)$ with

$$B_J(x) = \frac{2J+1}{2J}\coth\left(\frac{2J+1}{2J}x\right) - \frac{1}{2J}\coth\left(\frac{1}{2J}x\right),$$
$$x = \frac{g\mu_B JB}{k_B T}, \quad k_B = 0.086\,\frac{\text{meV}}{\text{K}}, \quad \mu_B = 0.058\,\frac{\text{meV}}{\text{T}}. \tag{24}$$

This equation is useful for several reasons. It shows the relative magnitude of the thermal and magnetic excitations, gives an example of a smooth interpolating function between the low- and high-temperature limits, and allows to study the high-temperature limit analytically. By expanding the function

$$B_J(x) \overset{T\to\infty}{\sim} \frac{J+1}{3J}x, \quad M_z \overset{T\to\infty}{\sim} \frac{N_A\mu_B^2}{3k_B}\frac{J(J+1)g^2B}{T}, \tag{25}$$

we arrive at the simple asymptotic form

$$\chi_M T(T) \overset{T\to\infty}{\sim} \frac{N_A\mu_B^2}{3k_B}J(J+1)g^2 \simeq 0.125\langle J^2\rangle g^2\,\frac{\text{cm}^3\text{K}}{\text{mol}}, \tag{26}$$

where the cgs-emu units adopted in experiment are used (Table I).

Finally, we mention that while the magnetic susceptibility measurement is a versatile approach to get information about (theoretically) all magnetic excited states regardless of their symmetry, fine details, especially about the energetic position of low-spin states, can be obscured by the thermodynamic averaging, viz. Eq. (18). In contrast, inelastic neutron scattering (INS) and electron paramagnetic resonance (EPR) experiments have a more direct access to the excited states, however, they are restricted by the selection rules: ΔS, $M_s = 0, \pm 1$ for INS, and $\Delta S = 0$ for EPR [4,64].

III. BARE METALLIC CLUSTER

A general strategy of performing calculations involving TM atoms is to converge an electronic state of highest multiplicity and use partially occupied natural orbitals as a basis for *multireference* self-consistent field and correlated calculations. In the $FeNi_4$ cluster, Fe and Ni atoms are in the oxidation state zero and possess valence electronic configurations s^2d^6 and s^1d^9, respectively. The highest possible multiplicity is 9. It is prohibitively hard to include all the $5\times(1+5)=30$ valence states in the active space. That is the reason why early calculations of magnetic anisotropies in TM clusters inevitably exploited the tight-binding approach [65,66].

Two mechanisms for the orbital ordering were considered here for the reduction of the configuration space: weak Ni-Ni versus weak Fe-Ni coupling. In the former case, depending on which Fe d orbital is doubly populated, a number of closely spaced electronic states arise. They differ by the orbital orderings on the Ni atoms. The energy spacing between different Fe d states is considerably larger. Our calculations, however, disproved this hypothesis and showed that, in fact, the second scenario takes place: the energy spacing between different orbital orderings on Ni atoms is larger than that of the Fe d states. The d orbital of Fe follows standard symmetry considerations for the crystal field splitting in the square planar geometry (Fig. 5) that minimizes overlap with

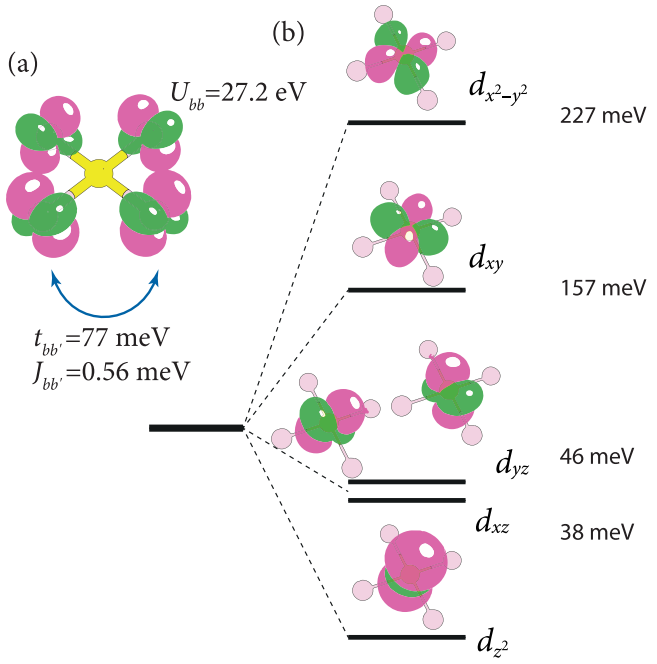

FIG. 5. Ordering of atomic orbitals in the $FeNi_4$ cluster. Spin-polarized natural atomic orbitals localized on Ni and Fe atoms are depicted in (a) and (b), respectively. They constitute the active space. The Hamiltonian matrix elements relevant for the antiferromagnetic coupling of Ni atoms are indicated in (a). In accordance with the Hamitonian (8), indices associated with the central atom are denoted as a, and for the peripheral atoms we use b, b', etc. The state averaged calculation performed in CAS(10,9) yields the crystal field splitting in (b).

the Ni d states. The orbitals are filled according to Hund's rule. Correspondingly, the d_{z^2} orbital is filled in the ground state, and the others are half-filled.

This finding allows us to simplify the calculations considerably: only one d state on each Ni atom plus four or five states on Fe need to be included in the active space (Fig. 5). We thus use the CAS self-consistent field (CASSCF) method with N active electrons in M active orbitals [CAS(N,M)] and perform the following sequence of calculations: (i) CAS(8,8) for the spin multiplicity $\kappa = 9$ followed by the multireference EOM-CC yielding 1, 4, 6, 4, 1 states in the multiplicities 1 to 9, respectively, Fig. 6(a); (ii) state-averaged CAS(10,9) for $\kappa = 9$ yielding five high-spin states; they serve as a basis for the multireference EOM-CC, predicting $5\times(1,4,6,4,1)$ states in all multiplicities in accordance with combinatorial considerations for the spin-1/2 flips on four sites and spin-2 rotation on the central site, Fig. 6(b). Finally, the spin-orbit and spin-spin interactions are added on top of (ii), Fig. 6(c). Computational details are presented in Appendix A. All the calculations were performed in a slightly distorted geometry in order to avoid degenerate states and make the rhombohedral splitting visible. They are well converged showing all the expected symmetry properties.

Having all the states at our disposal, we compute the magnetic susceptibility for (i) and (ii), Fig. 7. At first we notice that the energy splittings are substantial (for instance, the singlet state is 531 meV above the ground nonet state, i.e., a

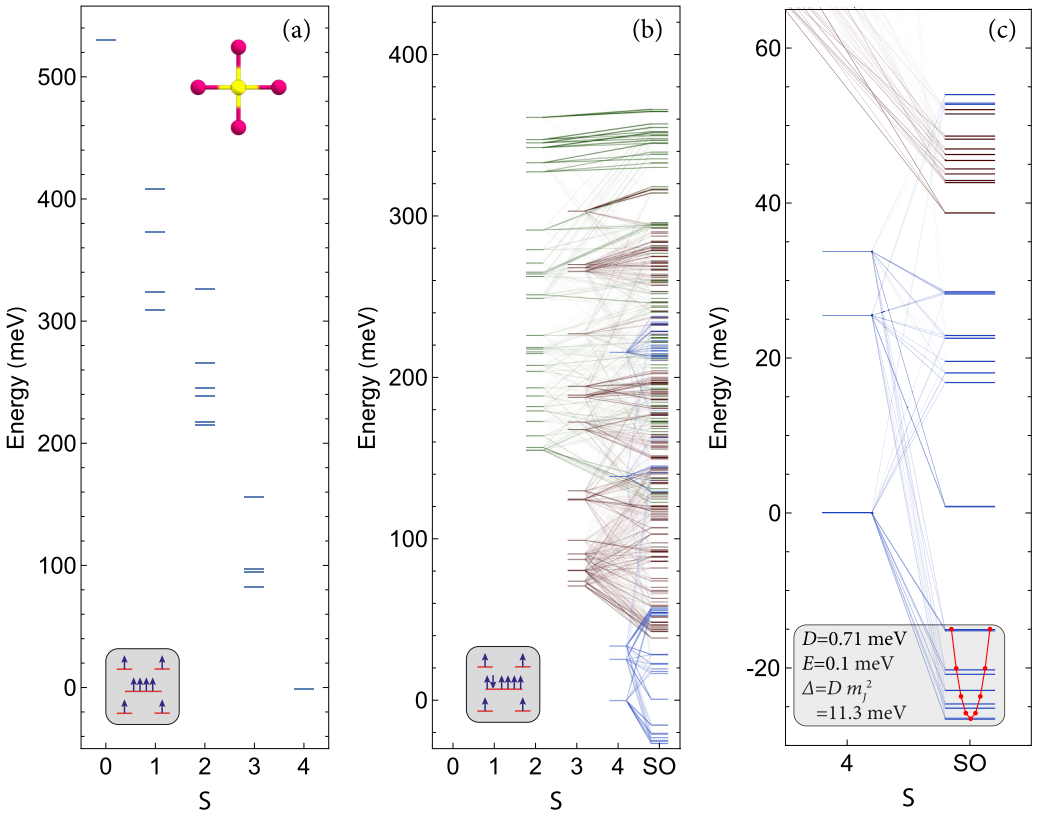

FIG. 6. Electronic states of the $FeNi_4$ cluster. (a) and (b) differ by the choice of reference spaces [CAS(8,8) and CAS(10,9) as depicted on the insets below]. (c) is a enlarged portion of the (b) showing spin-orbit splitting of the lowest energy spin multiplet. The strength of spin-orbit and spin-spin couplings is encoded in the width of lines connecting non- and relativistic calculations. The selection rule that $\langle aS_aM|\hat{\mathcal{H}}_{\rm SOC}|bS_bM'\rangle$ is different from zero only for $S_a - S_b = 0, \pm 1$ [cf. Eq. (2)] is manifested in the fact that each relativistic state is predominantly composed of states with the same spin, i.e., $S_a = S_b$ with a small admixture of $S_a - S_b = \pm 1$. There are no states composed of $S_a = 4$ and $S_b = 2$ at the same time. On the inset of (c), we compare the computed energy fine structure with the eigenenergies of the ZFS Hamiltonian (28) using the computed value of the axial parameter D and neglecting the rhombohedral splitting.

state with multiplicity 9). This explains why the saturated value of $\chi_M T(T)$ is reached at very high temperatures. We fit both susceptibilities using the eigenstates of the spin model, Eq. (14) with $s_A = 2$ and $s_B = 1/2$. In the CAS(8,8) case, both the *ab initio* and the model Hamiltonians possess the same set of states and multiplicities. Therefore the mapping is well justified yielding a rather large ferromagnetic Fe-Ni coupling, and a much smaller antiferromagnetic coupling between Ni atoms: $J_1 = 26.0$ meV, $J_2 = -4.4$ meV. It is interesting that naive application of Eq. (7) with $S_{\rm HS} = 4$, $S_{\rm LS} = 0$, and $\Delta_{\rm S} = 0$ (as suggested by Ruiz *et al.* [67,68] based on the broken symmetry approach) yields a very similar value of $J_1 = 26.6$ meV. One can substantiate the mapping onto the two-center model by regarding all four Ni atoms as one unit with the effective spin $S_B = 2$.

Because of the vanishing overlap between the d orbitals on the Fe and Ni atoms, a direct mechanism is the only explanation of the ferromagnetic coupling. In order to arrive at this conclusion, we use the Goodenough-Kanamori rule that superexchange interactions are of AFM type where the virtual electron transfer is between half-filled orbitals, but of FM type if the transfer is from a half-filled to an empty orbital or, as is the case here, from a filled (Fe-d_{z^2}) to half-filled d_{xz}, d_{yz} orbitals on the Ni atoms. We further notice that FM superexchange is a higher-order process, which can be neglected in the presence of strong direct interactions.

In contrast, the antiferromagnetic coupling between Ni atoms is a typical example of the kinetic exchange. It arises from the electron hopping between the half-filled Ni d orbitals (with matrix element $t_{bb'}$) and can be expressed as $J_2 = -2t_{bb'}^2/U_{bb}$, where $U_{bb} = U_{b'b'}$ is the on-site repulsion. This is a well known result of the degenerate perturbation theory where singlet and triplet ground states are coupled with matrix element $\sqrt{2}t_{bb'}$ to a charge transfer state with excitation energy U_{bb}. In order to verify the correctness of this interpretation, we performed an exact diagonalization (ED) on the CAS(8,8) subspace in undistorted geometry. In this way, we completely neglect the dynamic correlations, i.e., the virtual electron excitations outside of the active space are unaccounted for, but have the advantage that all matrix elements can be analyzed. Such an analysis is extremely useful for large systems where other correlated methods are not at our disposal. Importantly, the many-body Hamiltonian on the active subspace represents a very useful simplification of the full problem. In the discussion of Sec. II B, the relevance of the hopping mediated by ligands was emphasized. The magnitude of these matrix elements would be difficult to estimate from first principles. In the reduced Hamiltonian, they are present and account for all

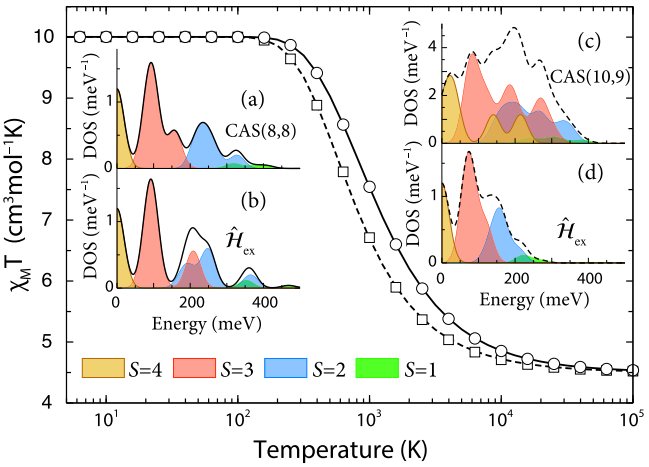

FIG. 7. The magnetic susceptibility of the $FeNi_4$ cluster computed using states from Fig. 6(a) (CAS(8,8) reference, circles), and Fig. 6(b) (CAS(10,9) reference, squares) and fitted by the spin model (8) with $s_A = 2$ and $s_B = 1/2$, full and dashed lines, respectively. The low and the high-temperature limits are consistent with $\langle S^2\rangle_0 = 20$ and $\langle S^2\rangle_\infty = 69/8$, Eqs. (22) and (23). Insets (a) and (b) compare the density of states from *ab initio* CAS(8,8) calculations and from the spin model, respectively. Analogically, insets (c) and (d) compare the density of states from *ab initio* CAS(10,9) calculations and from the spin model, respectively. The solid line denotes the total contribution from all spin multiplicities, whereas color-shaded curves separately resolve different spins. Notice a larger density in (c) because more states are included.

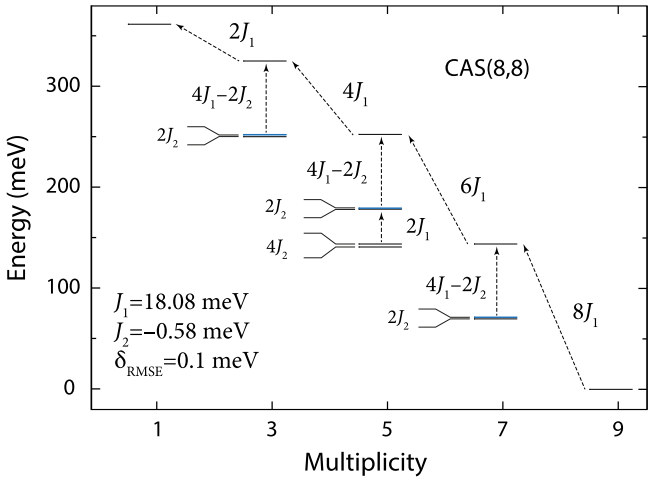

FIG. 8. Energy level scheme of the $FeNi_4$ cluster in an undistorted square geometry neglecting the dynamical correlations. Nondegenerate and doubly degenerate states are shown as black and blue lines, respectively. The expected level spacings from the exact solution (13) of the spin Hamiltonian (8) are indicated. Since the root-mean-square error of the fitting δ_{RMSE} is very small, eigenenergies of the *ab initio* and the spin model (4) are indistinguishable on the shown energy scale.

possible hopping pathways in a mean-field fashion. We will return to this point in the next section where a ligand-mediated scenario is considered.

For the current system, the situation is somewhat simpler because the hopping between Ni atoms ($t_{bb'}$) is direct and is not mediated by ligands. Other dominant matrix elements originating from the Coulomb interaction are indicated in Fig. 5(a). As becomes evident from Fig. 8, the results of ED using these matrix elements are perfectly matched by the spin model allowing to determine the exchange constants by the fitting of energy levels with accuracy exceeding 0.1 meV. In order to arrive at the same values of J_1 and J_2 perturbatively, the following has to be done.

(1) Account for the fact that J_{ab}—the exchange integral between different Fe and Ni states, Eq. (11)—depends on the type of the involved Fe d states. It can be easily demonstrated that J_1 is an average of these matrix elements: consider the splitting between states of multiplicity six and four arising from the exchange interaction of (composite) $S_B = 2$ and s_A according to the Hilbert space partition $2 \otimes \frac{1}{2} = \frac{3}{2} \oplus \frac{5}{2}$ and compare it with the interaction of constituent spins:

$$E_4 - E_6 = 5J_1 = 5J_{ab}. \tag{27}$$

For the second identity, we use the analytic solution (13) for the Hilbert space (14) with $J_2 = 0$.

(2) Account for the fact that J_2 is determined by the competition of the ferromagnetic exchange $J_{bb'} > 0$ and the kinetic exchange $-2t_{bb'}^2/U_{bb} < 0$.

Finally, we notice that electronic correlations beyond the conventional DFT are rarely discussed in the context of magnetic interactions in molecular systems. A comparison between the exchange constants obtained from the fitting of the $\chi_M T(T)$ curves, Fig. 7 (based on correlated excited states) and from the exact diagonalization on the subspace, Fig. 8, $J_1 = 26.0$ meV, $J_2 = -4.4$ meV versus $J_1 = 18.1$ meV, $J_2 = -0.58$ meV, indicates that the effect of electronic correlations is large and is particularly manifested when indirect mechanisms are present.

The extended CAS(10,9) calculation yields five times as many states related to the five possibilities of the doubly occupied d orbital in Fe. Due to this additional orbital degree of freedom, there could be no unique correspondence with the same spin model. There is some regularity in the spectra as, for instance, is evidenced by the replication of major peaks in the density of states depicted in Figs. 7(b) and 7(c), top panels. However, the majority of states has a mixed character with nonzero occupation probability of each of the Fe d states. This fact precludes a separate consideration of each subspace. Here, we can take advantage of the natural averaging provided by a thermodynamic quantity such as $\chi_M T(T)$ with a caveat that it gives a preferential treatment of high-spin states [the $S(S+1)$ factor in Eq. (21)]. The corresponding fit is likewise very accurate (cf. squares and dashed line in Fig. 7), however, the Ni-Ni exchange coupling is ferromagnetic now: $J_1 = 15.0$ meV, $J_2 = 4.8$ meV. Thus orbital degrees of freedom unaccounted for on the model Hamiltonian level distort the determination of exchange coupling constants. This finding substantiates the fact that $\chi_M T(T)$ being an integral thermodynamic quantity, i.e., such that it depends on the whole excitation spectrum, is insufficient to serve alone as a reliable method for the determination of exchange constants. A possible resolution of this ambiguity can involve a combination of experimental and theoretical investigations. Information about the excitation spectrum from, e. g., inelastic neutron

scattering can be exploited to improve the spin model by including the orbital degrees of freedom. One such study (albeit involving only spin degrees of freedom) has been performed recently by Furrer *et al.* [69].

On a smaller energy scale, relativistic effects are important although there is no strict separation of the scales set by (i) the crystal field splitting, (ii) the exchange interactions of spins, and (iii) the spin-orbit interaction as is evidenced by Fig. 6. If we take the spectral width due to the action of each of those effects, their magnitude can be estimated as 200 meV (Fig. 8), 500 meV [Fig. 6(a)], and 50 meV [Fig. 6(c)], respectively. Our calculations show that the spin-orbit splitting of the lowest nonet state is dominated by the interaction within the same spin-multiplets, the energy stabilization is around 26 meV. Only for higher energies the admixture of $\kappa = 7$ and 5 becomes important as can be seen in Fig. 6(b). We focus now on the lowest nonet [magnified in Fig. 6(c)] and characterize its splitting in terms of the effective zero-field splitting (ZFS) Hamiltonian:

$$\hat{\mathcal{H}}_D = D\left(\hat{S}_z^2 - \tfrac{1}{3}S(S+1)\right) + E\left(\hat{S}_x^2 - \hat{S}_y^2\right). \qquad (28)$$

The parameters of the ZFS Hamiltonian are our main finding for this molecule. The axial parameter D yields a well known ladder of states quantized with respect to the z-spin projection, whereas E additionally incorporates rhombohedral splitting. They can be related to the matrix elements of the $\mathbb{D}$ tensor discussed above [Eq. (4)]:

$$D = \mathbb{D}_{zz} - 1/2(\mathbb{D}_{xx} + \mathbb{D}_{yy}),$$
$$E = 1/2(\mathbb{D}_{xx} - \mathbb{D}_{yy}).$$

We predict a positive value of $D = 0.71$ meV, leading to a single-well parabolic potential [inset of Fig. 6(c)]. Thus, in this case, no quantum tunneling nor slow relaxation of magnetization can be observed. The rhombohedral parameter is very small ($E = 0.1$ meV). We note that these values almost entirely originate from spin-orbit effects—the contribution of spin-spin coupling is $D = 0.024$ meV.

As discussed in the context of Eq. (3), the latter contribution corresponds to the shape anisotropy (the dipole sum). In line with the data for magnetic anisotropies of thin films, it constitutes only a small but important fraction of the total value. Let us compare the computed values with the MAE of ultrathin Ni films on the Cu(001) surface. Ferromagnetic resonance measurements on this paradigmatic system were performed in 1994 by Schulz and Baberschke [40] and two reorientation transitions from the in-plane to out-of-plane and back to in-plane alignment of the magnetization vector as a function of the film thickness were found. It is of great technological importance to find materials with two distinct magnetic states: with large and negative D for SMM, and with large out-of-plane magnetization for films. Therefore the discovery of a possibility to control the easy axis of magnetization by varying the film thickness has stimulated a lot of experimental measurements [70,71] and theoretical calculations [72,73] for different substrates. For a monolayer Ni/Cu(001), the ferromagnetic resonance measurements of Schulz and Baberschke yielded for the energy difference between the out-of-plane and in-plane magnetization 124 μeV/atom ($E_\perp - E_\parallel = -K^{\text{eff}} = -(K_u^V + \frac{2K_u^S}{d})$, $K_u^V = 30\frac{\mu\text{eV}}{\text{atom}}$, $K_u^S = -77\frac{\mu\text{eV}}{\text{atom}}$, $d = 1$) [40]. A theoretical estimate by Bruno [41] using the tight-binding approach yielded a much larger value of 860 μeV/atom. This was subsequently improved by Moos *et al.* [32] using the degenerate perturbation theory. Their value for $E_\perp - E_\parallel$ is 120 μeV/atom, which includes the shape-anisotropy contribution of just 20 μeV/atom.

Summary. Our *ab initio* calculations demonstrate that the $FeNi_4$ cluster (i) possesses several important electronic and magnetic features that can be found in many larger organo-metallic complexes, and (ii) can serve as a paradigm for superexchange interactions in the presence of orbital degrees of freedom. Specifically, in this case, the kinetic exchange accounts for the interaction between Ni atoms. The full description thus requires a Hamiltonian of the type (6), which clearly goes beyond the considered model (8). Accurate fitting of the magnetization curves is still possible, however, it has to do with the "averaging" (in a thermodynamic sense) property of the susceptibility $\chi_M T(T)$. Working on a subspace of electronic states, i.e., explicitly excluding orbital degrees of freedom, allows to establish a correspondence to the model (8) individually for each state. Exchange constants can be reliably determined by fitting the energies to the model expressions, and are in agreement with the prediction of perturbation theory [53]. However, we find that electronic correlations significantly affect their values.

IV. ELECTRONIC PROPERTIES OF METALLACROWNS

Based on our insight from the study of the $FeNi_4$ cluster, we are now in the position to add ligands into the consideration. We use molecules that have been characterized structurally, electronically by XMCD, XAS, and magnetically by SQUID-magnetometry in works of Happ *et al.* [21,74]. The core molecule, which comprises the full salicylhydroxamic acid scaffold [Fig. 1(b,c)], has a chemical composition AB_4L_4, where A and B are transition metals, and L=$C_7H_4NO_3$ is the ligand complex. Accordingly, we consider cases A=Cu^{II}, B=Fe^{III} and A=Cu^{II}, B=Cu^{II}. The bond distances are very similar in both cases, the symmetry irreducible central region where magnetic exchange interactions are operative is depicted in Fig. 3. Both systems have in common that the magnetic $d_{x^2-y^2}$ orbital of the central Cu(II) ion directly points toward the linking donor atoms and is consequently capable to induce strong antiferromagnetic interactions.

For the two mentioned metallacrowns, we follow the same strategy for our first-principles calculations as outlined in Sec. III above. On the first step CASSCF in the highest possible multiplicity is performed using the def2-svp full electron basis set [75] of the double zeta quality and including the scalar relativistic effects on the second-order DKH level. SCF calculations are accelerated by the use of RIJCOSX method [76], which requires an exchange fitting basis [77]. On the second step the molecular orbitals from the active space are localized using the Boys procedure [78] and used as a basis for DMRG calculations. Dynamical correlations—in the sense of inclusion of virtual electron transitions in and out of the active space—are added on top of CASSCF where possible.

A. $CuCu_4$

Ab initio results for this homometallic metallacrown are summarized in Table II. CAS(5,5) predicts weakly AFM J_1 and

TABLE II. Energies of the {$CuCu_4$} MC in meV. Since the system is not of a perfect square geometry, the degeneracy is slightly lifted (these values are shown on the same line).

$\kappa = 2S+1$	Formula	CAS(5,5)	NEVPT2
2	$-2J_2$	1.798/1.798	4.748/4.773
2	$-2J_1+2J_2$	3.571	9.732
2	$-2J_1-2J_2$	7.191	17.308
4	J_1-4J_2	0.917	2.393
4	$-3J_1$	8.084	18.957
4	$-3J_1-2J_2$	9.894/9.894	23.370/23.407
6	$-4J_1-4J_2$	14.407	32.867

J_2 interactions. These values cannot be explained by the AFM superexchange alone. For an estimate, we can use matrix elements between the localized states from our calculations: the hopping parameters are $t_{bb'} = 165.88$, $t_{bb''} = 165.78$ meV and $t_{ab'} = t_{ab''} = 300.4$ meV, $U_{aa} = 28.79$ and $U_{bb} = 28.68$ eV from where the superexchange coupling can be deduced $J_{bb'} = J_{bb''} = -1.92$ and $J_{ab'} = J_{ab''} = -6.27$ meV (b, b', etc., denote symmetry-inequivalent peripheral Cu atoms). This significant difference to the CAS(5,5) results (listed in the third column of Table II) can be attributed to the act of other mechanisms including the direct ones.

Second-order perturbation theory (NEVPT2, see Appendix A for a summary of the used methods, Table IX) performed on top further increases the exchange interaction constants (forth column of Table II), however, they are almost three times smaller than the experimentally determined values ($J_1 = -19.24$ meV and $J_2 = -11.44$ meV [74]). Since this is the same trend (see Table III where results of different methods are compared with experiment) as was observed for the bare TM cluster, some clarifications are needed.

Consider the transition matrix element between the ground (gr) state and an excited charge transfer (CT) state in some abstract system. In the case of $FeNi_4$, this electronic transition is realized by a single-electron transition between two orbitals ϕ_b and $\phi_{b'}$ belonging to the active space. Properly accounting for the normalization of many-body wave functions [79] we arrive at $\sqrt{2}t_{bb'}$ as the transition matrix element between the many-body states. The charge transfer state in {$CuCu_4$} cannot be obtained by considering electronic transitions only within the active space. Let B and B' denote *atomic orbitals* predominantly constituting the b and b' TM *molecular orbitals*, respectively. The basic assumption is that they are half-filled and that the hopping $t_{BB'}$ vanishes because the magnetic ions are far apart. This is not so for $t_{bb'}$—the hopping between the molecular orbitals—as due to the hybridization with ligand-states it is no longer zero. Let us for definiteness assume that b and b' are obtained by the localization of molecular orbitals from the active space [such as depicted in Fig. 9(a)]. As can be seen from this plot, they contain a small admixture of the ligand p states:

$$\phi_b = \phi_B + \alpha_L \phi_L, \tag{29a}$$

$$\phi_l = \phi_L - \alpha_L \phi_B, \tag{29b}$$

where the collective index L denotes electronic states pertinent to ligand atoms. States (29a) and (29b) are orthonormal up to the first order in the hybridization coefficients α_L. Thereon we write explicitly the many-body ground and CT states as combinations of Slater determinants (denoted as $|\ldots|$)

$$\psi_{\rm gr}(S=0) = \frac{1}{\sqrt{2}}(|\phi_b\bar{\phi}_{b'}\phi_l| - |\bar{\phi}_b\phi_{b'}\phi_l|) + \psi_0^{(1)},$$

$$\psi_{\rm gr}(S=1, M_S=1) = |\phi_b\phi_{b'}\phi_l| + \psi_1^{(1)},$$

$$\psi_{\rm CT}^B = |\phi_b\bar{\phi}_b\phi_l| + \psi_B^{(1)},$$

where for simplicity we assume that there are no other magnetic d states in the active space and separate first-order corrections $\psi^{(1)}$ due to virtual transitions in and out of the active space. We follow the standard notation that $\bar{\phi}_b$ is a spin-flipped ϕ_b orbital. Now the hopping matrix element reads

$$\begin{aligned}&\langle\psi_{\rm CT}^B|\hat{t}|\psi_{\rm gr}(S=0)\rangle \\ &= \sqrt{2}(t_{BB'} + \alpha_{L'}t_{BL'} + \alpha_L t_{B'L}) \\ &\quad + 1/\sqrt{2}\langle\psi_B^{(1)}|\hat{t}|(|\phi_b\bar{\phi}_{b'}\phi_l| - |\bar{\phi}_b\phi_{b'}\phi_l|)\rangle + \langle|\phi_b\bar{\phi}_b\phi_l|\hat{t}|\psi_0^{(1)}\rangle.\end{aligned}$$

Here, $t_{BB'}$ vanishes by assumption, however, the two other terms in the first line are nonzero and are accounted for on the CASSCF level. By contrast, terms on the second line originate from virtual electron transitions outside the active space. These dynamical correlations can be taken into account perturbatively by, e.g., NEVPT2, or nonperturbatively with the help of multireference configuration interaction or coupled cluster methods. It is important to emphasize that both contributions are of the same order and cannot be neglected as the consideration of {$CuCu_4$} shows (Table III). We note in passing that ferromagnetic superexchange mechanism is a third-order effect [60,80], which is also partially covered by the CAS electronic states via the $\alpha_L\alpha_{L'}t_{BL}t_{L'B'}$ contributions.

TABLE III. The exchange interaction constants J_1 and J_2, the root-mean-square error $\delta_{\rm RMSE}$ of the least squares fitting at different levels of theory are compared with perturbative estimates according to the kinetic exchange mechanism (according to which $J_1 = -2t_{ab}^2/U_{aa}$ and $J_2 = -2t_{bb'}^2/U_{bb}$) and with experimental values. All values in meV.

Method	J_1	J_2	$\delta_{\rm RMSE}$
CAS(5,5)	−2.70	−0.90	0.00
NEVPT2	−6.36	−2.08	0.20
Kinetic exchange	−6.27	−1.92	
Experiment	−19.24	−11.44	

B. $CuFe_4$

It was demonstrated that a high-spin ground state ($S = 11/2$) in the $CuFe_4$ heterometallic metallacrown is realized by antiferromagnetic couplings of all five constituent TM atoms [21,74]. These findings can be compared with *ab initio* calculations. The minimal active space consistent with experimentally determined charges of transition metal atoms comprises all five d orbitals on the Fe^{III} ions and a single one on the central Cu^{II} ion. Self-consistent calculations in the highest-spin configuration ($S = 21/2$) of CAS(21,21)—21 electrons distributed over 21 d orbitals—indeed confirm that the half-filled Cu d orbital has in-plane orientation with lobes

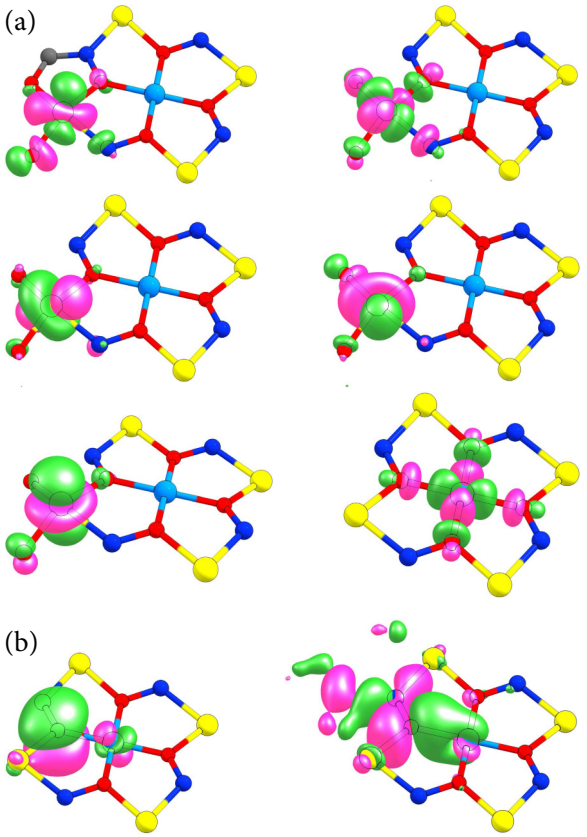

FIG. 9. The natural atomic orbitals on Fe and Cu atoms (a), and two representative localized MOs of the p character on the ligand atoms computed using the Boys procedure [78] (b).

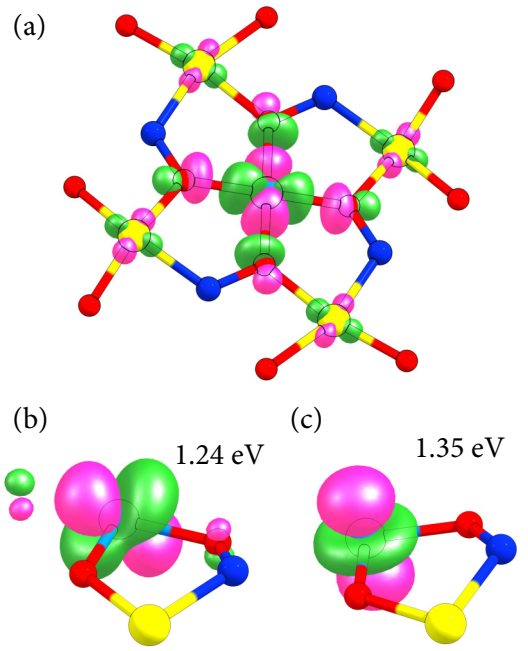

FIG. 10. The inclusion of different Cu d-MOs into the active space gives rise to different electronic states. Energy differences of the two excited states (b) and (c) with respect to the ground-state configuration (a) are indicated. All calculations are performed at the CAS(21,21) level of theory and the total spin $S = 21/2$.

pointing towards O atoms. Other orientations lead to a number of excited states with energies exceeding one eV (Fig. 10). This rather large energy difference explains why CAS(21,21) is sufficient, and why other d orbitals on the central Cu can be excluded from the active space.

However, CAS(21,21) is a rather large space motivating us to focus in more details on even smaller AB_2 units of the AB_4 cluster. The separation into subsystems is technically possible due to the use of a localized basis, Fig. 9. We perform DMRG calculations for two different scenarios where the Fe atoms are either nearest neighbors or are situated on a diagonal of the AB_4 cluster. These subsystems are depicted as insets of Fig. 11. The solution of the isosceles spin-triangle model (13) is used for fitting. A comparison of the two panels in Fig. 11 shows that J_1 exchange constant is drastically different for the two cases and the fit accuracy is lower in the nearest-neighbor case [panel (a)]. The latter finding hints at the deviation of the system's geometry from the ideal square shape. More information can be obtained by analyzing the matrix elements.

The data in Table IV demonstrate that the hopping between d orbitals is appreciable. As explained in the preceeding section, it results from nonzero hybridization coefficients α_L, Eqs. (29), and points at the importance of indirect mechanisms. Noticable is a strong variation of the hopping and the direct exchange depending on the orbital type of the same TM ion (these parameters are reported in columns 4 and 7). Since the molecule lacks fourfold symmetry, there are also smaller variations in the matrix elements pertinent to different atoms. Adding the distortion, i.e., introducing the δ asymmetry parameter (leading to the appearance of two different exchange constants $J_1' = (1-\delta)j$, $J_1'' = (1+\delta)j$) and using Eq. (12) instead of Eq. (13) for fitting, improves the agreement substantially (Table V), but does not change the conclusion of the analysis in Fig. 11 that the exchange constant J_1 is very different for the two subsystems. Notice

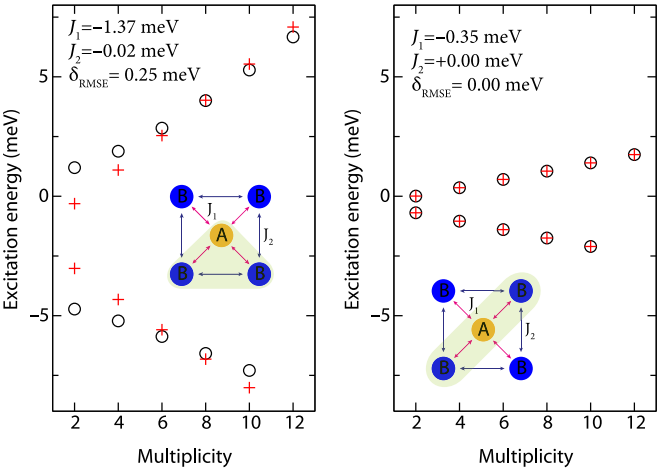

FIG. 11. Fitting of the DMRG calculations (circles) for two AB_2 subsystems (green shaded areas) of the $\{CuFe_4\}$ cluster with a spin model (8). The eigenvalues of the spin Hamiltonian corresponding to these isosceles triangles are shown as pluses. A large discrepancy in the fitted values of J_1 in the left vs right panels poses a question about the origin of the exchange coupling in this system.

TABLE IV. Averaged hopping and exchange matrix elements of the $\{CuFe_4\}$ molecule in meV. The averaging is performed for each pair of atoms (i, j) over all possible combinations of participating d orbitals ($i = 1, \ldots, 4$ for Fe^{III} ions and $i = 5$ for the central Cu^{II} ion). The variances $\mathrm{var}(a) = \langle (a - \langle a \rangle)^2 \rangle$ indicate how strongly these parameters of the many-body Hamiltonian deviate from the mean values $\langle a \rangle$. Additionally, we indicate the averaged superexchange coupling $J^{se} = -2\langle t^2 \rangle / U$.

Atoms		$\langle t_{ij} \rangle$	$\mathrm{var}(t_{ij})$	J_{ij}^{se}	$\langle J_{ij} \rangle$	$\mathrm{var}(J_{ij})$
1	2	128.8	104.0	−1.90	0.154	0.138
1	3	8.0	9.0	−0.01	0.001	0.001
2	3	123.6	120.4	−2.06	0.162	0.187
1	4	123.4	120.4	−2.06	0.162	0.187
2	4	8.3	8.2	−0.01	0.001	0.001
3	4	128.7	103.9	−1.90	0.155	0.138
1	5	184.6	153.7	−4.00	0.959	0.718
2	5	181.5	133.7	−3.52	0.887	0.601
3	5	184.6	153.7	−4.00	0.959	0.718
4	5	181.5	133.7	−3.52	0.887	0.601

that adding the biquadratic exchange interaction as explained in Appendix B does not improve the fitting in Fig. 11.

This indicates that in an AB_2 trimer, the exchange interactions J_1' and J_1'' are mutually dependent and that the difference between them cannot be attributed solely to the effect of the geometrical distortion on the hopping parameters. In order to elucidate the effect of other mechanisms, we perform calculations for (i) AB dimers, and AB_2 trimers with (ii) only A–B interactions, (iii) all possible pairwise interactions, and finally (iv) three- and four-center Coulomb integrals included. The results are presented in Fig. 12, panels (a), (b), (c), and (d), respectively. Demonstrably, the difference between all four scenarios is substantial. Only AB subsystems are well described by the sum of direct exchange and superexchange mechanisms, the corresponding estimates of the exchange constants are presented in columns 6 and 5 of Table IV, respectively. In AB_2 clusters, virtual electron transitions leading to the redistribution of the electronic occupations on different B atoms are mutually exclusive (in view of the Pauli principle) and the simple perturbative estimates in Table IV are no longer valid. The situation is even more complicated if we add all multicenter Coulomb integrals [panel (d)] to the case where only pairwise interactions are included [panel (c)]. The inclusion of these terms reduces the J_1 exchange constant by 38% in the linear cluster and doubles J_1'' in the triangular cluster. This is as well a manifestation of indirect exchange mechanisms. However, they cannot be reduced to the textbook application of the Anderson-Goodenough-Kanamori perturbative approach, which does not take into account the multicenter Coulomb integrals. Currently, there are no theories that account for multicenter integrals in superexchange interactions. Therefore first-principles calculations are indispensable for multicenter molecular magnets.

TABLE V. Results of the fitting of DMRG calculations for all possible AB_2 subsystems with the analytic solution (12). All exchange constants are in meV. The largest root-mean-square error of the fitting δ_{RMSE} is 10^{-4} meV. α and δ parameters are dimensionless and are defined as in Eq. (12). Data presented here are also visualized in Fig. 12(d).

B_1	B_2	j	J_1'	J_1''	J_2	α	δ
1	2	−1.253	−0.797	−1.709	−0.032	0.025	0.364
1	3	−0.350	−0.340	−0.350	0.000	−0.001	0.001
1	4	−1.296	−0.715	−1.878	−0.039	0.030	0.449
2	3	−1.296	−0.715	−1.878	−0.039	0.030	0.449
2	4	−0.285	−0.285	−0.285	0.000	−0.001	0.001
3	4	−1.253	−0.797	−1.709	−0.032	0.020	0.364

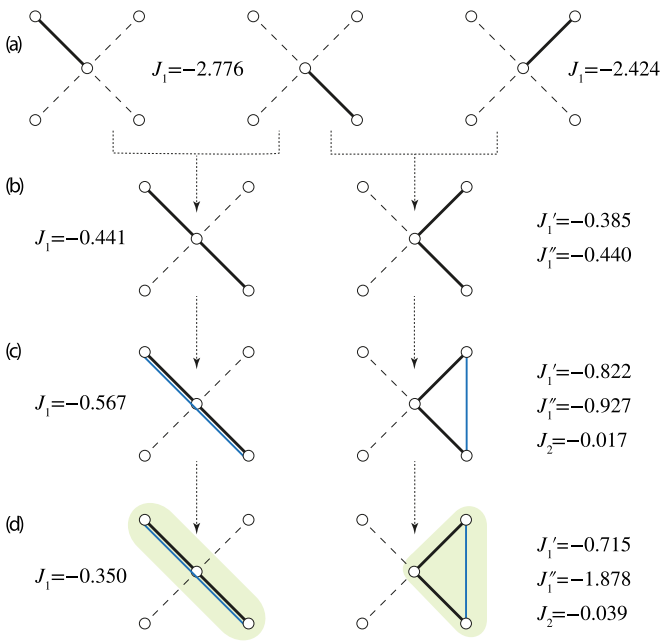

FIG. 12. Variation of the exchange constants in meV units for different included interactions within AB and AB_2 spin clusters of the $Cu^{II}(DMF)_2Cl_2[12{-}MC_{Fe^{III}N(Shi)} - 4](DMF)_4$ molecule. Thick lines denote the included hopping and pairwise Coulomb matrix elements—black for nearest and blue for next-nearest neighbors—whereas dashed lines stand for the excluded pairwise interactions. DMRG solutions of the cluster models are mapped onto the analytic solutions for spin dimers (a) and trimers [(b)–(d)]. The energy levels of an AB_2 cluster are given by Eq. (12) with $s_A = 1/2$ and $s_B = 5/2$.

Let us now focus on the electronic excitations of the whole AB_4 system. This is a very difficult task because the number of electronic configurations grows rapidly with decreasing multiplicity. That is why we computed excited states using the CASSCF(21,21) approach only for the two highest multiplicities and found that they differ by $E_{22} - E_{20} = 16$ meV. Such calculations account for static and, to some extent, dynamic correlations because different orbital relaxations for each spin multiplicity are permitted. Other states are possible to access only by the use of specialized methods such as DMRG albeit neglecting dynamical correlations (Table VII). It is very important that DMRG calculations are performed in the localized basis. While calculations are possible to converge in MO basis, they typically lead to excited states.

The fitting procedure, with the goal to determine values of the spin-exchange constants J_1 and J_2, is different from

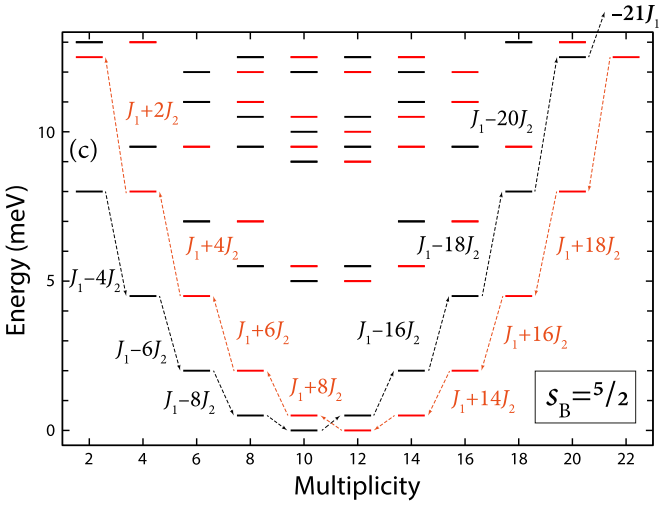

FIG. 13. Energy levels of the spin model (8) involving the Fe^{III} high-spin $s_B = 5/2$ configuration from the analytic solution (13). Black horizontal bars denote levels of the all-AFM setting ($J_1 < 0$, $J_2 < 0$), whereas red ones correspond to FM $J_1 > 0$ and AFM $J_2 < 0$ interactions. In order to emphasize symmetries between AFM and FM solutions, we use values of the exchange constants $J_1 = \pm 5.5$ meV and $J_2 = -0.5$ meV that only approximately correspond to the experimental exchange constants $J_1 = -6.10$ meV and $J_2 = -0.47$ meV ($s_B = 5/2$) [9]. The lowest energy state in each scenario (chosen as reference) is a frustrated magnetic configuration with intermediate total spin.

the one used for the $\{CuCu_4\}$ MC and for AB and AB_2 subclusters of the $\{CuFe_4\}$ MC above. The dimension of the Hilbert space of the spin model—it contains 286 different spin multiplets (15c)—is prohibitively large to perform the fitting on the totality of states. Thus a subset of well identifiable states needs to be selected. It seems that the lowest-energy states in each multiplicity serve well this purpose. With the analytical solution of the spin Hamiltonian given by Eq. (13) (lowest part of the spectrum is shown in Fig. 13), we additionally assume that both exchange constants are antiferromagnetic in order to choose expressions for fitting. One hint for such an assumption comes from the $\chi_M T(T)$ measurements of Happ and Rentschler [74]. Another indication is that a fully ferromagnetic configuration with $\kappa = 22$ is strongly disfavored on the CASSCF and DMRG levels, cf. last row of Table VII with the energy level scheme in Fig. 13. On the other hand, experimental results for other systems containing Cu and Fe ions (Table VI) show that interaction between these ions can also be of ferromagnetic type. The interplay of different indirect mechanisms, which are very system-specific, is a decisive factor. We also note in passing that for the Heisenberg spin model the low-temperature limit of the magnetic susceptibility

TABLE VII. Energies of the $\{CuFe_4\}$ MC with respect to the lowest doublet ($\kappa = 2$) state in meV. Analytic solution (13) is tabulated in the second column. Generic energy level schemes corresponding to FM and AFM couplings are visualized in Fig. 13. Results of the least squares fitting are compared with experimental values in Table VIII.

$\kappa = 2S + 1$	Formula	DMRG(21,21)
4	$J_1 - 4J_2$	−0.5181
6	$2J_1 - 10J_2$	−0.9533
8	$3J_1 - 18J_2$	−1.2928
10	$4J_1 - 28J_2$	−1.5337
12	$5J_1 - 40J_2$	−1.6751
14	$6J_1 - 54J_2$	−1.7165
16	$7J_1 - 70J_2$	−1.6446
18	$8J_1 - 88J_2$	−1.4980
20	$9J_1 - 108J_2$	−1.2370
22	$-12J_1 - 108J_2$	14.4791

TABLE VI. Some systems containing magnetically interacting Fe and Cu ions. Here, Tp stands for hydrotris (pyrazolyl) borate, bpca for bis(2-pyridylcarbonyl)amidate, and tacn for 1,4,7-triazacyclononane, dmg for dimethylglyoxime, bpb for bis(pyridine-2-carboxamido)benzenate, and tn for 1,3-propanediamine.

Material	Spin system	S_{Fe}	J_{Cu-Fe} (cm^{-1})	Ref.
$[(Dopn)Cu^{II}(OH_2)Fe^{III}(Cl)L](ClO_4)_2$	Dimer, six-coordinated Fe, distorted square pyramidal Cu with $d_{x^2-y^2}$ orbitals pointing towards bridging N and O, AFM σ-superexchange $d_{x^2-y^2} \parallel p(N) \parallel p(O) \parallel d'_{x^2-y^2}$ vs. FM $d_{x^2-y^2} \parallel p(N) \perp p(O) \parallel t'_{2g}$ pathway	5/2	−38.8	[81]
$[L_2Fe_2Cu(dmg)_3](ClO_4)_2 * 0.5MeOH$	Trimer, octahedral coordination of the two Fe^{III}	5/2	−42.0	[82]
$[Tp_2(Me_3tacn)_3Cu_3Fe_2(CN)_6]^{4+}$	Trigonal bipyramidal metal-cyanide core with approximate D_{3h} symmetry	1/2	+8.5	[83]
$[CuL1][Fe(bpb)(CN)_2]_2 * 4H_2O$	Cyano-bridged complex, AFM origin is not clear	1/2	−0.59	[84]
$[Cu(tn)_2][Fe(bpb)(CN)_2]_2 * 2H_2O$	Amino-bridged complex, FM coupling due to orthogonality of 3d magnetic orbitals between Cu(II) and Fe(III)	1/2	+3.1	[84]
$[(Tp)Fe(CN)_3Cu(Tp)]_2 * 2H_2O$	Tetranuclear square cluster, square pyramidal coordination of Cu	1/2	+11.9	[85]
$[(Tp)Fe(CN)_3Cu(bpca)]_2 * 4H_2O$	Tetranuclear square cluster, square pyramidal coordination of Cu, ZFS	1/2	+1.38	[85]

TABLE VIII. The exchange interaction constants J_1 and J_2, the root-mean-square error δ_{RMSE} of the least squares fitting involving lowest energy states in each multiplicity κ are shown in meV. The fully converged ground state is a frustrated magnetic configuration with the total spin $S = 13/2$. Experimental measurements yield $S = 11/2$ as the lowest energy state [74].

Method	J_1	J_2	δ_{RMSE}
DMRG(21,21)	−0.7476	−0.0507	0.0113
Experiment	−6.10	−0.47	

(21), which is determined by the ground-state multiplicity (22), and its high-temperature limit, which is obtained by assuming equal occupation probability for each of the states (23), are almost indistinguishable for the two scenarios when J_1 is ferro- or antiferromagnetic (see discussion in Sec. II C). This can immediately be seen from the spectrum in Fig. 13 and makes determination of J_1 and J_2 on the basis of $\chi_M T(T)$ rather challenging.

The results of fitting of the DMRG calculations (see Table VII) are as follows: (i) Similarly to the $\{CuCu_4\}$ system, the root-mean-square error δ_{RMSE} is in the range of 10 μeV indicating the high accuracy of the procedure and the relevance of the spin model. (ii) Unlike for the AB_2 subclusters, the rhombic distortion is small, the value of J_1 is greater than that for the linear AB_2 cluster and is smaller than for the triangular one. (iii) In comparison with experiment ($J_1 = -6.1$ meV and $J_2 = -0.47$ meV), both exchange constants are substantially underestimated ($J_1 = -0.75$ meV and $J_2 = -0.05$ meV). As our calculations for the $\{CuCu_4\}$ system suggest (Sec. IV A), these values can be improved by adding dynamical correlations. Such calculations go beyond current computational capabilities for the $\{CuFe_4\}$ system. It is interesting to notice, however, that the ratio J_1/J_2, which determines the ground state, is also well reproduced. We predict that $S = 13/2$ is the frustrated antiferromagnetic ground state, whereas the $S = 11/2$ state is just 0.04 meV above it. Experimentally, $S = 11/2$ is the state of lowest energy.

C. Summary

Superexchange magnetic interactions are typically treated perturbatively and require at least two virtual electron transitions (from two TM atoms to the bridging ligand atom). Therefore it is not immediately obvious and, to the best of our knowledge, was not demonstrated before that even the simplest AFM mechanism can be treated by the complete active space approach. In this section, we provided such mathematical argument and supported it by *ab initio* calculations. We found a very precise mapping onto the spin model is possible for the $\{CuCu_4\}$ system (Table III) and the $\{CuFe_4\}$ system (Table VIII). At the same time, the fitted exchange constants cannot be solely explained by the Anderson-Goodenough-Kanamori AFM superexchange mechanism. We performed a detailed study of the magnetic interactions in subclusters of the $\{CuFe_4\}$ system and found three- and four-center Coulomb integrals are important. We also show that the exchange constants are strongly modified by dynamical electron correlations. The latter effects can only partially be taken into account for the $\{CuCu_4\}$ system.

V. CONCLUSIONS

In this work, we presented quantum chemistry calculations of three transition metal clusters with progressively increasing complexity of electronic states. Dealing with multideterminant open-shell electronic states represents the main difficulty of the correlated calculations. Therefore we started with the complete active space approach followed, where possible, by the inclusion of dynamical correlations. Relativistic effects are added on the scalar-relativistic level via the DKH Hamiltonian, and on top of the excited state calculations by including spin-orbit and spin-spin coupling effects.

Mapping of the *ab initio* calculations onto spin-models was the main goal of our study. For $FeNi_4$ and $\{CuCu_4\}$ we find perfect correspondence on the lowest (CAS) level of theory. At the same time it is possible to establish (and even to make these conclusions quantitative) that the observed exchange splitting cannot be explained only with the help of direct and AFM su-

TABLE IX. *Ab initio* methods used in this work. In order to run CHEMPS2, we use interface provided by ORCA (CIstep DMRGCI option to CASSCF).

Key	Method	Note
RIJCOSX	Treatment the Coulomb term via the resolution of identity (RI) and the exchange term via seminumerical integration [76,91]	ORCA [24]
Trafostep RI	Integral transformation in CASSCF calculations using RI	
DKH	Douglas-Kroll-Hess relativistic Hamiltonian [27]	
DLPNO	Decomposition of Intermolecular Interaction Energies within the Local Pair Natural Orbital Coupled Cluster Framework [92] (option for NEVPT2)	
NEVPT2	N-Electron Valence State Perturbation Theory [93]	
dkh-def2-svp	Relativistically recontracted Karlsruhe basis sets [75]	
def/jk	Coulomb+Exchange fitting for all def2 basis sets [77]	
DoSOC, DoSSC	Spin-orbit, spin-spin couplings and ZFS calculations [36]	
DMRG	Density matrix renormalization group	CHEMPS2 [25]
NPA	Natural population analysis [94]	JANPA [95]

perexchange mechanisms. The Goodenough-Kanamori rules give only qualitative estimates. For $\{CuFe_4\}$, accurate mapping onto a spin model has been established for a set of lowest energy states in each multiplicity, which where obtained by the DMRG calculations.

Going beyond the CAS level of theory, we found that dynamical correlations are important. We arrive at this conclusion by generalizing the AFM exchange mechanism to the CAS reference states and showing that virtual electron transitions outside the active space are of comparable magnitude. This is further supported by *ab initio* calculations.

The determination of J_1 and J_2 parameters is also an important experimental goal. For the two metallacrowns, they were determined by fitting the temperature dependence of the magnetic susceptibility. While this is generally accepted and a very reliable method, examples of the bare metallic $FeNi_4$ cluster and the $\{CuFe_4\}$ metallacrown show that, due to inherent thermodynamical averaging, the results of such an approach are not unique and should be supported by the spectroscopical measurements, e.g., inelastic neutron scattering.

Relativistic effects are important on the smaller energy scale where the mapping onto the effective ZFS Hamiltonian was performed (accurate nonrelativistic calculations is a prerequisite). For the bare $FeNi_4$ cluster, we find $D = 0.71$ meV predominantly due to the spin-orbit coupling. While the axial parameter is positive precluding the observation of the spin tunneling of magnetization in this system, the absolute value is large. This finding encourages further explorations of metallacrowns possessing this interesting phenomenon.

In a recent comprehensive review [86] focusing on the rigorous extraction of magnetic Hamiltonians, major challenges for theoretical methods are presented and possible solutions are discussed. Here, we would like to put our results in a broader context of new trends of molecular magnetism. An important goal in molecular magnetism is to control the intramolecular exchange coupling. For storage purposes, the exchange coupling should be maximized in order to stabilize the magnetic state at finite temperature, while for quantum computing applications the exchange coupling must be easily switchable by external means. As Neese and Pantazis point out [87], a lot of synthetic efforts for the development of more efficient single molecule magnets is put into the maximization of the total spin. However, this does not automatically imply the maximization of the magnetic relaxation barrier. Instead, there seems to be a number of systems where high axial anisotropy is achieved through electronic configurations with close to orbital degeneracy, which maximizes spin-orbit interaction and leads to large zero-field splitting. The importance of orbital degrees of freedom was emphasized already in an early work of Bruno [41]: "there is a very strong connection between the anisotropy energy and the orbital moment." Thus future developments will certainly pursue the route of optimization of magnetic properties through the optimization of ligands. A complementary and universal approach for the design of magnetic systems with desired properties is via an external driving field. Ultrafast and reversible control of the exchange interaction iron oxides [88] has recently been demonstrated. Theoretical foundations for the driven spin systems were set in recent letters [89,90]. We anticipate even more developments in this direction.

ACKNOWLEDGMENT

This work is supported by the German Research Foundation (Deutsche Forschungsgemeinschaft, DFG) Collaborative Research Center SFB/TRR 173 "Spin+X".

APPENDIX A: COMPUTATIONAL DETAILS AND *AB INITIO* METHODS REFERENCE

All calculations were performed using the def2-svp full electron basis set [75] of the double zeta quality and including the scalar relativistic effects on the second-order DKH level (see Table IX for a summary of the used *ab initio* methods). It results in 205, 901, and 901 contracted basis functions for the $FeNi_4$ cluster, $\{CuCu_4\}$ and $\{CuFe_4\}$ metallacrowns, respectively. Geometry optimization was performed for the model $FeNi_4$ cluster, whereas experimental geometries are used for the metallacrown molecules. Correlated calculations for the $FeNi_4$ cluster were performed in the energy window from -5 to 5 Hr, i.e., molecular orbitals in the range from 26 to 147 were correlated. Reference configurations with weight above the $t_{\rm pre} = 10^{-4}$ threshold were selected, and the convergence criteria $E_{\rm tol} = 10^{-7}$ and $R_{\rm tol} = 10^{-7}$ were used.

APPENDIX B: BIQUADRATIC EXCHANGE INTERACTION IN AB2 SPIN CLUSTERS

For spin-1/2 systems, the biquadratic spin-exchange is reduced to the ordinary exchange by the virtue of the identity:

$$(\hat{\mathbf{s}}_i \cdot \hat{\mathbf{s}}_j)^2 = \tfrac{3}{16} - \tfrac{1}{2}\hat{\mathbf{s}}_i \cdot \hat{\mathbf{s}}_j. \tag{B1}$$

Thus this mechanism is only nontrivially manifest in the interaction of larger spins. It turns out, however, that such renormalization of ordinary exchange constants by the biquadratic exchange is more common. Consider a spin-dimer AB, where $s_A = \frac{1}{2}$, but s_B is arbitrary. Using the same method as in Ref. [62], here we have

$$(\hat{\mathbf{s}}_A \cdot \hat{\mathbf{s}}_B)^2 = \frac{1}{4}s_B(s_B+1) + \frac{i}{2}\sum_{jkl}\epsilon_{jkl}\hat{s}_A^{(j)}\hat{s}_B^{(k)}\hat{s}_B^{(l)},$$

where j, k, and l are running over three projections, and ϵ_{jkl} is the fully antisymmetric tensor. From the commutation relation of the spin-operators on the same site

$$\left[\hat{s}_B^{(k)},\hat{s}_B^{(l)}\right] = i\epsilon_{jkl}\hat{s}_B^{(j)},$$

we obtain

$$(\hat{\mathbf{s}}_A \cdot \hat{\mathbf{s}}_B)^2 = \tfrac{1}{4}s_B(s_B+1) - \tfrac{1}{2}\hat{\mathbf{s}}_A \cdot \hat{\mathbf{s}}_B. \tag{B2}$$

From this equation immediately follows that for the isosceles spin-triangle model (AB_2) the biquadratic exchange Hamiltonian $\hat{\mathcal{H}}_{\rm ex}^{(2)}$ commutes with the exchange Hamiltonian $\hat{\mathcal{H}}_{\rm ex}$ [cf. Eqs. (8) and (9)]. As a consequence, the A-B exchange constant is modified as $J_1 \to J_1 - 1/4\kappa_1$, whereas κ_2 additionally contributes:

$$-\tfrac{1}{2}\kappa_2\left[S_B(S_B+1) - s_{B_1}(s_{B_1}+1) - s_{B_2}(s_{B_2}+1)\right]^2, \tag{B3}$$

to the total energy. Here, $\hat{\mathbf{S}}_B = \hat{\mathbf{s}}_{B_1} + \hat{\mathbf{s}}_{B_2}$.

[1] J. Simon, W. S. Bakr, R. Ma, M. E. Tai, P. M. Preiss, and M. Greiner, Quantum simulation of antiferromagnetic spin chains in an optical lattice, Nature (London) **472**, 307 (2011).

[2] A. O. Leonov and M. Mostovoy, Multiply periodic states and isolated skyrmions in an anisotropic frustrated magnet, Nat. Commun. **6**, 8275 (2015).

[3] Olivier Kahn, *Molecular Magnetism* (VCH, New York, NY, 1993).

[4] A. Furrer and O. Waldmann, Magnetic cluster excitations, Rev. Mod. Phys. **85**, 367 (2013).

[5] Myoung Soo Lah and V. L. Pecoraro, Isolation and Characterization of $\{Mn^{II}[Mn^{III}(salicylhydroximate)]_4(acetate)_2(DMF)_6\}$: An Inorganic Analog of M^{2+}(12-crown-4), J. Am. Chem. Soc. **111**, 7258 (1989).

[6] G. Lefkidis, *Ab initio investigation of 12-membered* Mn-N-O_4 *ether-metallacrown*, Diploma Thesis, Aristotle University of Thessaloniki, 1994.

[7] G. Mezei, C. M. Zaleski, and V. L. Pecoraro, Structural and Functional Evolution of Metallacrowns, Chem. Rev. **107**, 4933 (2007).

[8] M. Tegoni and M. Remelli, Metallacrowns of copper(II) and aminohydroxamates: Thermodynamics of self assembly and host-guest equilibria, Coord. Chem. Rev. **256**, 289 (2012).

[9] P. Happ, C. Plenk, and E. Rentschler, 12-MC-4 metallacrowns as versatile tools for SMM research, Coord. Chem. Rev. **289-290**, 238 (2015).

[10] A. Athanasopoulou, C. Gamer, L. Völker, and E. Rentschler, Metallacrowns reaching the nanosize regime, in *Novel Magnetic Nanostructures: Unique Properties and Applications*, edited by E. Rentschler, N. Domracheva, and M. Caporali (Elsevier, Amsterdam, 2018).

[11] Jonathan R. Friedman, M. P. Sarachik, J. Tejada, and R. Ziolo, Macroscopic Measurement of Resonant Magnetization Tunneling in High-Spin Molecules, Phys. Rev. Lett. **76**, 3830 (1996).

[12] W. Wernsdorfer, Quantum Phase Interference and Parity Effects in Magnetic Molecular Clusters, Science **284**, 133 (1999).

[13] D. Gatteschi and R. Sessoli, Quantum tunneling of magnetization and related phenomena in molecular materials, Angew. Chem., Int. Ed. **42**, 268 (2003).

[14] C. M. Ramsey, E. del Barco, S. Hill, S. J. Shah, C. C. Beedle, and D. N. Hendrickson, Quantum interference of tunnel trajectories between states of different spin length in a dimeric molecular nanomagnet, Nat. Phys. **4**, 277 (2008).

[15] E. Burzurí, F. Luis, O. Montero, B. Barbara, R. Ballou, and S. Maegawa, Quantum Interference Oscillations of the Superparamagnetic Blocking in an Fe 8 Molecular Nanomagnet, Phys. Rev. Lett. **111**, 057201 (2013).

[16] Yiming Chen, M. D. Ashkezari, C. A. Collett, R. A. Allão Cassaro, F. Troiani, P. M. Lahti, and J. R. Friedman, Observation of Tunneling-Assisted Highly Forbidden Single-Photon Transitions in a Ni_4 Single-Molecule Magnet, Phys. Rev. Lett. **117**, 187202 (2016).

[17] S. J. Blundell, Molecular magnets, Contemp. Phys. **48**, 275 (2007).

[18] L. Bogani and W. Wernsdorfer, Molecular spintronics using single-molecule magnets, Nat. Mater. **7**, 179 (2008).

[19] J. R. Friedman and M. P. Sarachik, Single-Molecule Nanomagnets, Annu. Rev. Condens. Matter Phys. **1**, 109 (2010).

[20] S. Carretta, T. Guidi, P. Santini, G. Amoretti, O. Pieper, B. Lake, J. van Slageren, F. El Hallak, W. Wernsdorfer, H. Mutka, M. Russina, C. J. Milios, and E. K. Brechin, Breakdown of the Giant Spin Model in the Magnetic Relaxation of the Mn_6 Nanomagnets, Phys. Rev. Lett. **100**, 157203 (2008).

[21] P. Happ, A. Sapozhnik, J. Klanke, P. Czaja, A. Chernenkaya, K. Medjanik, S. Schuppler, P. Nagel, M. Merz, E. Rentschler, and H. J. Elmers, Analyzing the enforcement of a high-spin ground state for a metallacrown single-molecule magnet, Phys. Rev. B **93**, 174404 (2016).

[22] G. A. Craig, J. J. Marbey, S. Hill, O. Roubeau, S. Parsons, and M. Murrie, Field-Induced Slow Relaxation in a Monometallic Manganese(III) Single-Molecule Magnet, Inorg. Chem. **54**, 13 (2015).

[23] R. Boča, Zero-field splitting in metal complexes, Coord. Chem. Rev. **248**, 757 (2004).

[24] F. Neese, The ORCA program system, Wiley Interdiscip. Rev.: Comput. Mol. Sci. **2**, 73 (2012).

[25] S. Wouters, W. Poelmans, P. W. Ayers, and D. Van Neck, CheMPS2: A free open-source spin-adapted implementation of the density matrix renormalization group for ab initio quantum chemistry, Comput. Phys. Commun. **185**, 1501 (2014).

[26] J. E. Harriman, *Theoretical Foundations of Electron Spin Resonance*, Physical Chemistry Vol. 37 (Academic Press, New York, 1978).

[27] B. Sandhoefer and F. Neese, One-electron contributions to the g-tensor for second-order Douglas-Kroll-Hess theory, J. Chem. Phys. **137**, 094102 (2012).

[28] R. McWeeny, *Methods of Molecular Quantum Mechanics*, 2nd ed., Theoretical Chemistry (Academic Press, London, 1992).

[29] P. Bruno, Dipolar magnetic surface anisotropy in ferromagnetic thin films with interfacial roughness, J. Appl. Phys. **64**, 3153 (1988).

[30] Klaus Baberschke, Anisotropy in Magnetism, in *Band-Ferromagnetism*, Vol. 580, edited by R. Beig, J. Ehlers, U. Frisch, K. Hepp, W. Hillebrandt, D. Imboden, R. L. Jaffe, R. Kippenhahn, R. Lipowsky, H. v. Löhneysen, I. Ojima, H. A. Weidenmüller, J. Wess, J. Zittartz, Klaus Baberschke, Wolfgang Nolting, and Markus Donath (Springer Berlin Heidelberg, Berlin, Heidelberg, 2001) pp. 27–45.

[31] Thorsten Moos, *Elektronische Theorie für den Urpsrung der magnetischen Anisotropieenergie von Fe- und Ni-Monolagen*, Master's thesis, Freie Universität Berlin, Berlin (1995).

[32] T. H. Moos, W. Hübner, and K. H. Bennemann, Magnetocrystalline anisotropy energy of a transition metal monolayer: A non-perturbative theory, Solid State Commun. **98**, 639 (1996).

[33] M. Farle, A. Berghaus, and K. Baberschke, Magnetic anisotropy of Gd (0001)/W (110) monolayers, Phys. Rev. B **39**, 4838 (1989).

[34] J. Nogués and I. K. Schuller, Exchange bias, J. Magn. Magn. Mater. **192**, 203 (1999).

[35] F. Hellman, A. Hoffmann, Y. Tserkovnyak, G. S. D. Beach, E. E. Fullerton, C. Leighton, A. H. MacDonald, D. C. Ralph, D. A. Arena, H. A. Dürr, P. Fischer, J. Grollier, J. P. Heremans, T. Jungwirth, A. V. Kimel, B. Koopmans, I. N. Krivorotov, S. J. May, A. K. Petford-Long, J. M. Rondinelli, N. Samarth, I. K. Schuller, A. N. Slavin, M. D. Stiles, O. Tchernyshyov, A. Thiaville, and B. L. Zink, Interface-induced phenomena in magnetism, Rev. Mod. Phys. **89**, 025006 (2017).

[36] F. Neese, Calculation of the zero-field splitting tensor on the basis of hybrid density functional and Hartree-Fock theory, J. Chem. Phys. **127**, 164112 (2007).

[37] C. van Wüllen, Magnetic anisotropy from density functional calculations. Comparison of different approaches: Mn_{12} O_{12} acetate as a test case, J. Chem. Phys. **130**, 194109 (2009).

[38] Sebastian Schmitt, Patrick Jost, and Christoph van Wüllen, Zero-field splittings from density functional calculations: Analysis and improvement of known methods, J. Chem. Phys. **134**, 194113 (2011).

[39] H. J. Elmers and U. Gradmann, Magnetic anisotropies in Fe (110) films on W (110), Appl. Phys. A **51**, 255 (1990).

[40] B. Schulz and K. Baberschke, Crossover from in-plane to perpendicular magnetization in ultrathin Ni/Cu(001) films, Phys. Rev. B **50**, 13467 (1994).

[41] Patrick Bruno, Tight-binding approach to the orbital magnetic moment and magnetocrystalline anisotropy of transition-metal monolayers, Phys. Rev. B **39**, 865 (1989).

[42] A. Lessard, T. H. Moos, and W. Hübner, Magnetocrystalline anisotropy energy of transition-metal thin films: A nonperturbative theory, Phys. Rev. B **56**, 2594 (1997).

[43] Y. Tokura and N. Nagaosa, Orbital physics in transition-metal oxides, Science **288**, 462 (2000).

[44] See W. Hübner *et al.* [96] and references therein.

[45] T. Soda, Y. Kitagawa, T. Onishi, Y. Takano, Y. Shigeta, H. Nagao, Y. Yoshioka, and K. Yamaguchi, Ab initio computations of effective exchange integrals for H-H, H-He-H and Mn_2 O_2 complex: Comparison of broken-symmetry approaches, Chem. Phys. Lett. **319**, 223 (2000).

[46] J. Hubbard, Electron Correlations in Narrow Energy Bands, Proc. R. Soc. London A **276**, 238 (1963).

[47] W. Hübner and L. M. Falicov, Theory of spin-polarized electron-capture spectroscopy in ferromagnetic nickel, Phys. Rev. B **47**, 8783 (1993).

[48] Chi-Cheng Lee, H. C. Hsueh, and Wei Ku, Dynamical linear response of TDDFT with LDA+U functional: Strongly hybridized Frenkel excitons in NiO, Phys. Rev. B **82**, 081106 (2010).

[49] L. M. Falicov and R. H. Victora, Exact solution of the Hubbard model for a four-center tetrahedral cluster, Phys. Rev. B **30**, 1695 (1984).

[50] R. H. Victora and L. M. Falicov, Exact Solution of a Four-Site d-electron Problem: The Nickel-Metal Photoemission Spectrum, Phys. Rev. Lett. **55**, 1140 (1985).

[51] A. Palii, B. Tsukerblat, S. Klokishner, K. R. Dunbar, J. M. Clemente-Juan, and E. Coronado, Beyond the spin model: Exchange coupling in molecular magnets with unquenched orbital angular momenta, Chem. Soc. Rev. **40**, 3130 (2011).

[52] *Correlated Electrons: From models to materials; lecture notes of the Autumn School 2012 at Forschungszentrum Jülich 3-7 September 2012*, Schriften des Forschungszentrums Jülich Reihe Modeling and Simulation No. 2, edited by E. Pavarini and Institute for Advanced Simulation (Forschungszentrum Jülich, Jülich, 2012).

[53] P. W. Anderson, Antiferromagnetism. Theory of superexchange interaction, Phys. Rev. **79**, 350 (1950).

[54] J. B. Goodenough, An interpretation of the magnetic properties of the perovskite-type mixed crystals $La_{1-x}Sr_xCoO_{3-\lambda}$, J. Phys. Chem. Solids **6**, 287 (1958).

[55] J. Kanamori, Superexchange interaction and symmetry properties of electron orbitals, J. Phys. Chem. Solids **10**, 87 (1959).

[56] J. B. Goodenough, *Magnetism and the Chemical Bond*, Interscience Monographs on Chemistry: Inorganic Chemistry Section (Interscience Publishers, New York, 1963).

[57] C. Kittel, Model of Exchange-Inversion Magnetization, Phys. Rev. **120**, 335 (1960).

[58] K. Penc, N. Shannon, and H. Shiba, Half-Magnetization Plateau Stabilized by Structural Distortion in the Antiferromagnetic Heisenberg Model on a Pyrochlore Lattice, Phys. Rev. Lett. **93**, 197203 (2004).

[59] K. Iida, S.-H. Lee, T. Onimaru, K. Matsubayashi, and T. J. Sato, Determination of spin Hamiltonian in the Ni 4 magnetic molecule, Phys. Rev. B **86**, 064422 (2012).

[60] P. W. Anderson, New Approach to the Theory of Superexchange Interactions, Phys. Rev. **115**, 2 (1959).

[61] Nai Li Huang and R. Orbach, Biquadratic Superexchange, Phys. Rev. Lett. **12**, 275 (1964).

[62] D. Chaudhuri, G. Lefkidis, and W. Hübner, All-spin-based ultrafast nanologic elements with a Ni_4 cluster, Phys. Rev. B **96**, 184413 (2017).

[63] J. T. Haraldsen, T. Barnes, and J. L. Musfeldt, Neutron scattering and magnetic observables for S = 1/2 spin clusters and molecular magnets, Phys. Rev. B **71**, 064403 (2005).

[64] P. L. Scott and C. D. Jeffries, Spin-lattice relaxation in some rare-earth salts at helium temperatures; observation of the phonon bottleneck, Phys. Rev. **127**, 32 (1962).

[65] G. M. Pastor, J. Dorantes-Dávila, S. Pick, and H. Dreyssé, Magnetic Anisotropy of 3d Transition-Metal Clusters, Phys. Rev. Lett. **75**, 326 (1995).

[66] J. Dorantes-Dávila and G. M. Pastor, Magnetic Anisotropy of One-Dimensional Nanostructures of Transition Metals, Phys. Rev. Lett. **81**, 208 (1998).

[67] E. Ruiz, J. Cano, S. Alvarez, and P. Alemany, Broken symmetry approach to calculation of exchange coupling constants for homobinuclear and heterobinuclear transition metal complexes, J. Comput. Chem. **20**, 1391 (1999).

[68] E. Ruiz, A. Rodríguez-Fortea, J. Tercero, T. Cauchy, and C. Massobrio, Exchange coupling in transition-metal complexes via density-functional theory: Comparison and reliability of different basis set approaches, J. Chem. Phys. **123**, 074102 (2005).

[69] A. Furrer, A. Podlesnyak, and K. W. Krämer, Extraction of exchange parameters in transition-metal perovskites, Phys. Rev. B **92**, 104415 (2015).

[70] H. J. Elmers, J. Hauschild, H. Höche, U. Gradmann, H. Bethge, D. Heuer, and U. Köhler, Submonolayer Magnetism of Fe (110) on W (110): Finite Width Scaling of Stripes and Percolation Between Islands, Phys. Rev. Lett. **73**, 898 (1994).

[71] H. J. Elmers, J. Hauschild, H. Fritzsche, G. Liu, U. Gradmann, and U. Köhler, Magnetic Frustration in Ultrathin Fe Films, Phys. Rev. Lett. **75**, 2031 (1995).

[72] X. Qian and W. Hübner, First-principles calculation of structural and magnetic properties for Fe monolayers and bilayers on W (110), Phys. Rev. B **60**, 16192 (1999).

[73] T. Andersen and W. Hübner, Substrate effects on surface magnetism of Fe/W(110) from first principles, Phys. Rev. B **74**, 184415 (2006).

[74] P. Happ and E. Rentschler, Enforcement of a high-spin ground state for the first 3d heterometallic 12-metallacrown-4 complex, Dalton Trans. **43**, 15308 (2014).

[75] F. Weigend and R. Ahlrichs, Balanced basis sets of split valence, triple zeta valence and quadruple zeta valence quality for H to Rn: Design and assessment of accuracy, Phys. Chem. Chem. Phys. **7**, 3297 (2005).

[76] R. Izsák and F. Neese, An overlap fitted chain of spheres exchange method, J. Chem. Phys. **135**, 144105 (2011).
[77] F. Weigend, Hartree-Fock exchange fitting basis sets for H to Rn, J. Comput. Chem. **29**, 167 (2008).
[78] C. Edmiston and K. Ruedenberg, Localized atomic and molecular orbitals, Rev. Mod. Phys. **35**, 457 (1963).
[79] See detailed explanation in the Appendix II of Ref. [53].
[80] H. Kramers, L'interaction Entre les Atomes Magnétogènes dans un Cristal Paramagnétique, Physica **1**, 182 (1934).
[81] F. Birkelbach, M. Winter, U. Floerke, H.-J. Haupt, C. Butzlaff, M. Lengen, E. Bill, A. X. Trautwein, K. Wieghardt, and P. Chaudhuri, Exchange Coupling in Homo- and Heterodinuclear Complexes Cu^{ii} M [M = Cr(III), Mn(III), Mn(II), Fe(III), Co(III), Co(II), Ni(II), Cu(II), Zn(II)]. Synthesis, Structures, and Spectroscopic Properties, Inorg. Chem. **33**, 3990 (1994).
[82] P. Chaudhuri, M. Winter, P. Fleischhauer, W. Haase, U. Flörke, and H.-J. Haupt, A novel series of heterotrinuclear complexes with a tris(dimethylglyoximato)metal(II) anion as bridging ligand. Structure of the Fe^{iii} Cu^{ii} Fe^{iii} complex with S= 9/2 ground state, J. Chem. Soc., Chem. Commun. **0**, 1728 (1990).
[83] Cai-Feng Wang, Jing-Lin Zuo, B. M. Bartlett, Y. Song, J. R. Long, and Xiao-Zeng You, Symmetry-Based Magnetic Anisotropy in the Trigonal Bipyramidal Cluster $[Tp_2(Me_3tacn)_3 Cu_3 Fe_2(CN)_6]^{4+}$, J. Am. Chem. Soc. **128**, 7162 (2006).
[84] Bing Zhang, Zhong-Hai Ni, Ai-Li Cui, and Hui-Zhong Kou, Heterometallic trinuclear Cu^{ii} M_2^{iii} (M = Fe or Cr) complexes with novel bridges and unusual magnetic properties, New J. Chem. **30**, 1327 (2006).
[85] Wei Liu, Cai-Feng Wang, Yi-Zhi Li, Jing-Lin Zuo, and Xiao-Zeng You, Structural and Magnetic Studies on Cyano-Bridged Rectangular Fe_2 M_2 (M = Cu, Ni) Clusters, Inorg. Chem. **45**, 10058 (2006).
[86] J. P. Malrieu, R. Caballol, C. J. Calzado, C. de Graaf, and N. Guihéry, Magnetic Interactions in Molecules and Highly Correlated Materials: Physical Content, Analytical Derivation, and Rigorous Extraction of Magnetic Hamiltonians, Chem. Rev. **114**, 429 (2014).
[87] F. Neese and D. A. Pantazis, What is not required to make a single molecule magnet, Faraday Discuss. **148**, 229 (2011).
[88] R. V. Mikhaylovskiy, E. Hendry, A. Secchi, J. H. Mentink, M. Eckstein, A. Wu, R. V. Pisarev, V. V. Kruglyak, M. I. Katsnelson, Th. Rasing, and A. V. Kimel, Ultrafast optical modification of exchange interactions in iron oxides, Nat. Commun. **6**, 8190 (2015).
[89] A. P. Itin and M. I. Katsnelson, Effective Hamiltonians for Rapidly Driven Many-Body Lattice Systems: Induced Exchange Interactions and Density-Dependent Hoppings, Phys. Rev. Lett. **115**, 075301 (2015).
[90] M. Bukov, M. Kolodrubetz, and A. Polkovnikov, Schrieffer-Wolff Transformation for Periodically Driven Systems: Strongly Correlated Systems with Artificial Gauge Fields, Phys. Rev. Lett. **116**, 125301 (2016).
[91] F. Neese, F. Wennmohs, A. Hansen, and U. Becker, Efficient, approximate and parallel Hartree-Fock and hybrid DFT calculations. A 'chain-of-spheres' algorithm for the Hartree-Fock exchange, Chem. Phys. **356**, 98 (2009).
[92] Yang Guo, K. Sivalingam, E. F. Valeev, and F. Neese, SparseMaps—A systematic infrastructure for reduced-scaling electronic structure methods. III. Linear-scaling multireference domain-based pair natural orbital N-electron valence perturbation theory, J. Chem. Phys. **144**, 094111 (2016).
[93] C. Angeli, R. Cimiraglia, S. Evangelisti, T. Leininger, and J.-P. Malrieu, Introduction of n-electron valence states for multireference perturbation theory, J. Chem. Phys. **114**, 10252 (2001).
[94] A. E. Reed, R. B. Weinstock, and F. Weinhold, Natural population analysis, J. Chem. Phys. **83**, 735 (1985).
[95] T. Y. Nikolaienko, L. A. Bulavin, and D. M. Hovorun, JANPA: An open source cross-platform implementation of the Natural Population Analysis on the Java platform, Comput. Theor. Chem. **1050**, 15 (2014).
[96] W. Hübner, Y. Pavlyukh, G. Lefkidis, and J. Berakdar, Magnetism of a four-center transition-metal cluster revisited, Phys. Rev. B **96**, 184432 (2017).